SUPPLEMENT TO RADIATION SHIELDING ANALYSES OF JOYO-(C)

FEBRUARY, 1982

POWER REACTOR AND NUCLEAR FUEL DEVELOPMENT CORPORATION

HITACHI Ltd.

PNC-TJ 202 82-03
Feb. 1982

Supplement to Radiation Shielding Analyses of JOYO - (C) *

Ryoichi Kondo**
Takeshi Ozawa**
Junnosuke Horie***
Hiroyuki Handa***

* This work was performed under the contracts between Power Reactor and Nuclear Fuel Development Corporation and Hitachi Ltd.

** Hitachi Works, Hitachi Ltd.

*** Hitachi Engineering Company

ABSTRACT

A supplemental study on the JOYO's shielding analysis was performed focussing attention on the behavior of neutron and gamma-ray fluxes around the detector guide tube of channel A and on the evaluation of the primary sodium activation with use made of the two-dimensional discrete ordinates transport code.

It has been found out that secondary gamma rays emitted from a thin guide tube material of SS-304 has a strong effect of enhancing gamma dose rates in the guide tube penetrating through a graphite shielding. The effect of the guide tube penetrating a heavy concrete pedestal has been revealed to be a streaming of neutrons and gammas. It can be concluded that the effect of the detector guide tube on the neutron and gamma ray should be taken into account when comparing the calculated values with experimental values.

The neutron flux distribution in the full reactor lower axial two dimensional geometry has been calculated and used, together with the results obtained by the upper axial two dimensional analysis, to evaluate the primary sodium activity due to sodium-24 and -22. The calculated activity is about a factor of two higher than that of measurement. As for the evaluation of the sodium activity, more detail investigation of the neutron flux and the activation cross section of sodium should be performed in the future.

TABLE OF CONTENTS

CHAPTER 1

INTRODUCTION

1.1 Initiation of the supplemental analysis

When the full reactor shielding analysis of JOYO (see Fig.1.1.1) was performed by using the two dimensional discrete ordinates transport code, DOT 3.5, the results were compared with the experimental quantities such as ^{235}U fission rates, Cu neutron capture rates, total and thermal fluxes and gamma ray dose rates. The comparison showed that the analytical results were almost satisfactory and proved that the two dimensional discrete ordinates code is effective for analyzing the shielding performance for the full reactor bulky system. There were, however, great underestimations in the neutron flux and gamma ray dose rate particulary at positions where two dimensional geometry description could not be applied. One of these was the neutron and gamma ray fluxes in the detector guide tube of Channel A of which location is shown in Figs. 1.1.2 and 1.1.3. This guide tube, composed of SS-304, penetrates a heavy concrete pedestal downwards to a voided space below the pedestal and again penetrates a graphite shield downwards to 100 cm below the core midplane.

The calculated neutron fluxes at positions corresponding the penetration path of the guide tube were about two times the measured fluxes. While the calculated gamma ray dose rates at the same location were factors of 0.03 to 0.1 smaller than the measured dose rates. At that time, the difference in the gamma dose rates were thought to attribute to the lack of consideration of the secondary gamma ray emitted from the stainless steel neutron capture.

Along the penetration path in the heavy concrete pedestal, the computational to experimental values were, at the worst, of the order of 10^{-3} for the thermal neutron flux, and about a tenth for the gamma ray dose rates. There is a nitrogen space under the pedestal. The neutrons and gamma rays in the reactor vessel well stream into this region. Therefore, it

was expected that neglecting the streaming effect due to the guid tube penetration might lead to a great difference in the computational to experimental values.

Then it was needed to investigate what the effect is that the guide tube penetration has on the neutron and gamma ray flux.

One of the most important shielding data is the sodium activity because the shielding for the primary coolant activity may determine the size of plant. In JOYO the sodium activity has been being measured since reactor startup. Considering the importance of the sodium activity it was needed to evaluate an accuracy of predicting the sodium activity using the result of our shielding analysis method.

1.2 Summary of problem analyzed

As was mentioned in the preceding section, the primary objective of this study is to evaluate the effect of the detector guide tube and to evaluate the primary sodium activity in JOYO. Each evaluation has several calculational approaches and problems. In this section we will briefly summarize problems analyzed in this study.

The detector guide tube locates at an outer region of the reactor system as seen in Fig. 1.1.2. This situation introduce problem as to whether it is possible to evaluate the effect of the guide tube, which requires the three dimensional geometrical configuration, by using the two dimensional discrete ordinates transport calculation. The neutron and gamma ray behavior depends on where guide tube exists. Therefore we devided the analysis of the guide tube effect into three calculational steps.

First we need to know whether it is adequate to use the two dimensional transport code to analyze the flux distribution actually in three dimensional

geometry. This analysis is performed without considering exisitence of the guide tube penetration.

Next we substitute the graphite region by the voided region and SS-304 region in order to model the guide tube. This calculation is used for analyzing the effect of the guide tube on the neutron and gamma ray in the graphite shield.

Then we calculate the neutron and gamma ray fluxes at the guide tube penetrating the heavy concrete pedestal. In this calculation we need to consider the obliquity of the guide tube, which requires the adjustment of boundary angular fluxes.

We will apply simple analytical methods of usual form to predict the gamma ray flux at the guide tube in the graphite shielding and the neutron and gamma ray fluxes streaming through the guide tube in the pedestal.

When the previous shielding analysis was initiated attention was fixed on the radiation flux distribution in full reactor upper axial geometry. Then the analysis was performed by modeling the reactor above the core mid-plane. In order to predict the sodium activity we need the neutron flux distribution in all the regions of the reactor which contains sodium. Therefore, the first step of predicting the sodium activity is to perform the full reactor lower axial two dimensional transport calculation. Then the results of this calculation together with those by the previous analysis are directly used to predict the sodium activity.

In the following chapters we will describe these analyses in detail and discuss the results in comparison with shielding data measured.

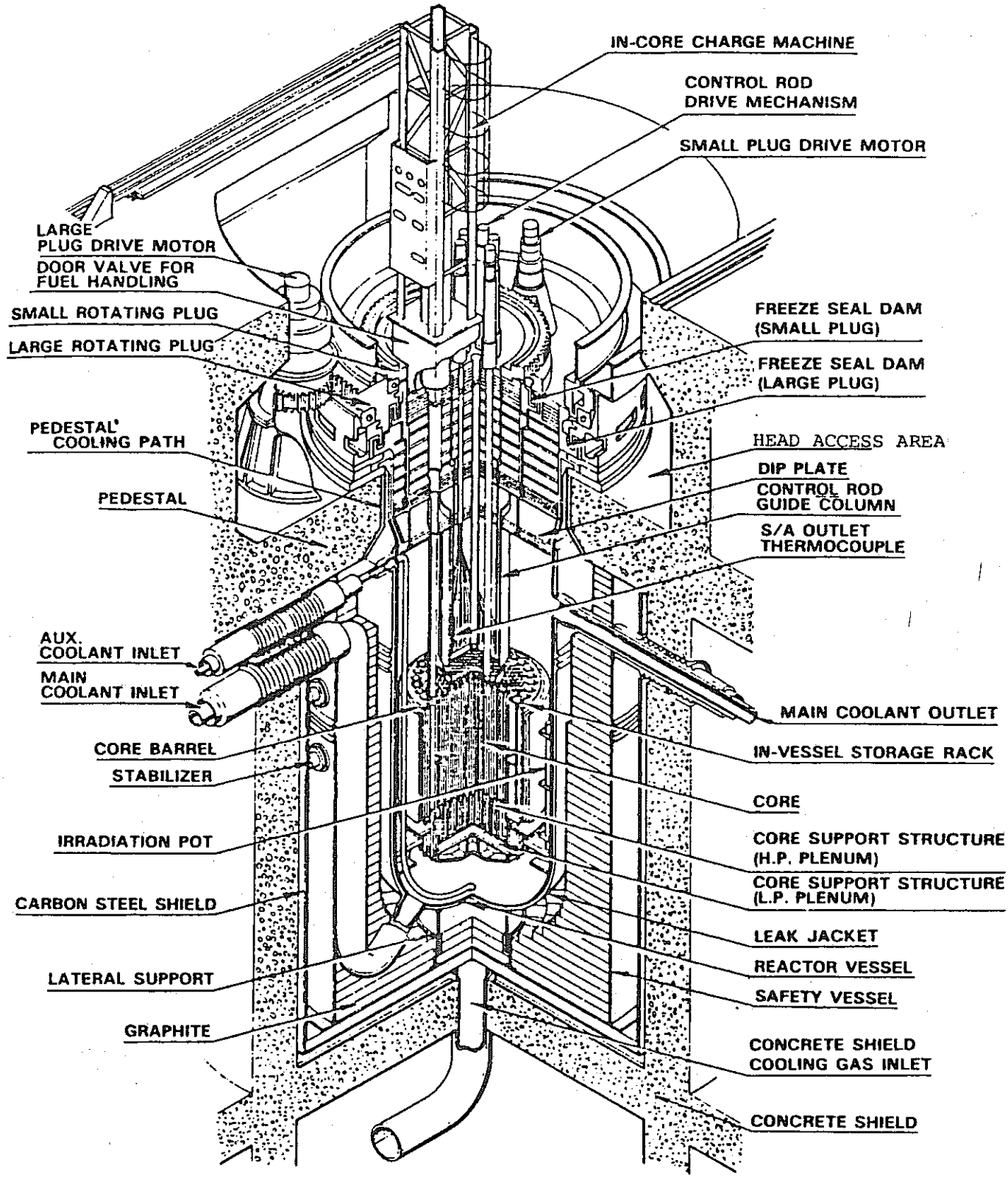

Fig. 1.1.1 JOYO reactor system.

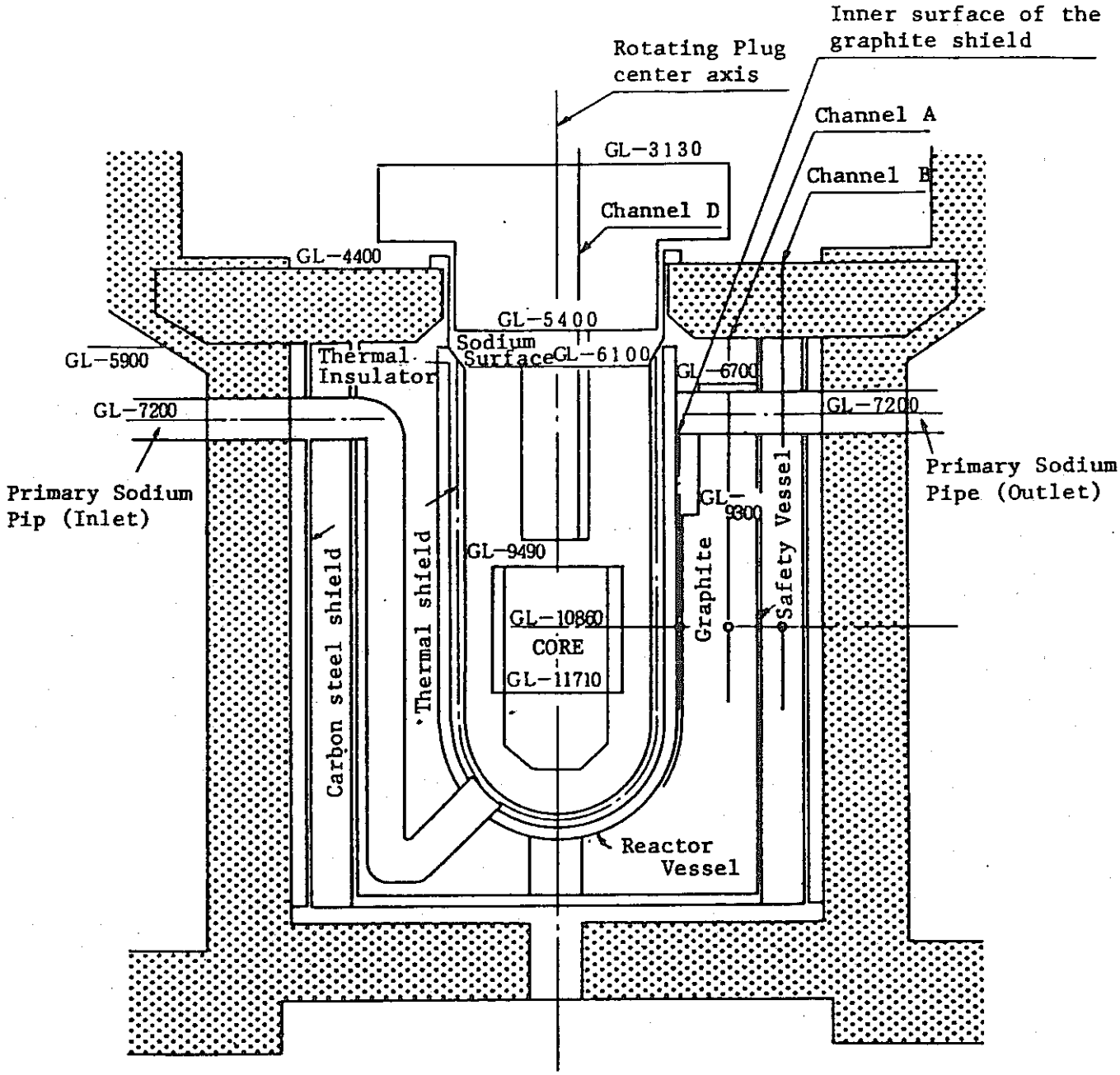

Fig. 1.1.2 Conceptual vertical cross section of JOYO and measured positions.

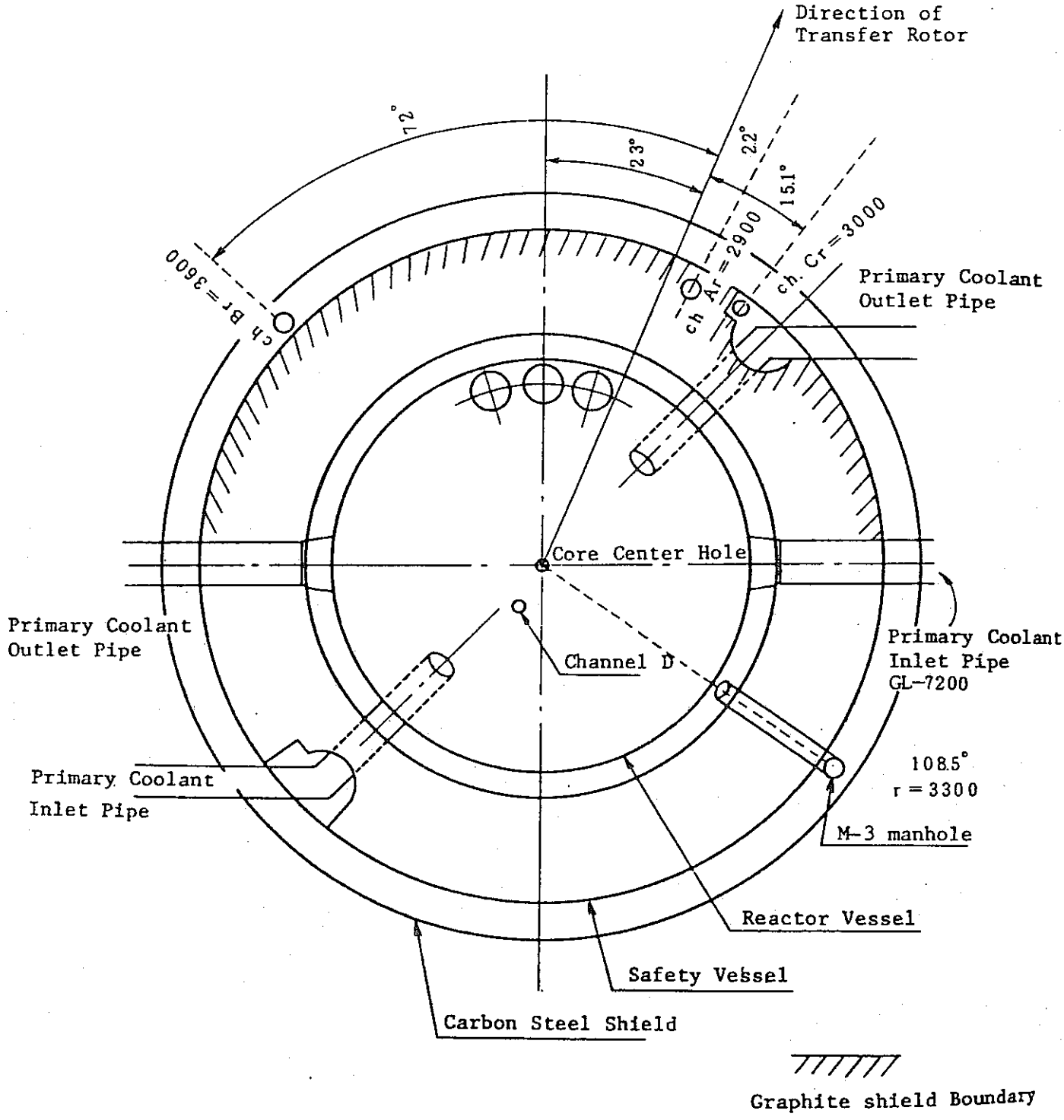

Fig.1.1.3 Conceptual horizontal cross section of JOYO and measured positions.

CHAPTER 2

ANALYSIS OF EFFECT OF DETECTOR GUIDE TUBE ON NEUTRON FLUX AND GAMM RAY DOSE RATE

2.1 Detector guide tube penetration in the graphite shield

The primary objective of this section is to investigate the effect that the guide tube has on the neutron flux and the gamma ray dose rate in the graphite shield region. As was already described in the previous chapter, we had to investigate an applicability of the approximation of describing the actual three dimensional geometry by two dimensional model. This study was performed without considering the existence of the guide tube penetration and is referred to as case 1 study. Then the graphite region was substituted by voids and SS-304 in order to include the penetration region. This is referred to as case 2 study. The domain used in this study is shown in Fig.2.1.1 with the dashed line which includes the guide tube penetration. From this figure we can easily see which domain was picked up from the full reactor analysis.

2.1.1 Calculational model

The geometry is common both for case 1 and for case 2 study and is shown in Fig.2.1.2 with the regions identified in Table 2.1.1. The region extended from a level of core mid-plane to the lower part of the concrete pedestal. A center axis of this R-Z geometry corresponds to a position 290 cm from the core center axis. The radius of this R-Z model is 27.5 cm. The spatial mesh intervals in the axial direction and materials used are the same as those of the full reactor upper axial model.

In order to calculate the flux distribution in this approximate model the boundary angular flux was used on the right boundary. The boundary flux is the outward angular flux at radius of 262.5 cm in the full reactor analysis. Table 2.1.2 summarizes the calculational parameters used in case 1 and 2 studies. The energy group structure and the S-120 angular quadrature, which was a specially developed asymmetric one, are respectively shown in Tables 2.1.3 and 2.1.4.

In case 2 study an inner radius of the guide tube is 7.5 cm and an outer radius 8.26 cm. The nitrogen region outside the guide tube extends to a radius of 11.25 cm.

2.1.2 Calculational results

(1) Case 1 study

The neutron flux and gamma ray dose rate contours of this case are shown in Figs. 2.1.3 through 2.1.6. These figures in turn represent the fast, intermediate and thermal neutron fluxes, and the gamma ray dose rate. In these figures, contour lines between 10^n and $10^{⑤-n+1}$ are for 2×10^n and 5×10^n. Note that the material used in regions 1 through 4 designated in Fig. 2.1.2 is the graphite. These results were compared with those of the full reactor analysis and showed that the neutron fluxes and gamma ray dose rate are as about twice as larger than those of the full reactor analysis at positions corresponding to the detector guide tube. This is reasonable since the incoming fluxes are assumed uniform around the radial boundary in case 1 model, while the actual incoming fluxes are not uniform and exist almost on half the radial boundary only. We can find a peculiar behavior of the gamma ray dose rate in Fig. 2.1.6. This is because of the higher secondary gamma ray production due to the thermal neutron than in the full reactor model. Considering that we focus our attention primarily on the effect of the secondary gamma ray due to the guide tube and that the gamma ray production cross section of SS-304 is much larger than that of graphite, we can easily expect that the peculiar behavior of the gamma ray dose rate in case 1 model dose not affect on the analysis based on case 2 model.

(2) Case 2 Study

Figs. 2.1.7 through 2.1.10 show the neutron flux and gamma ray dose rate contours of this case which includes the guide tube penetration model. By comparison with the results of the previous case 1 study which neglects the guide tube model, it is seen that the fast and intermediate neutron fluxes are flattened in the guide tube penetration and their flux levels are slightly (about a factor of two) higher than those of case 1 along the guide tube. This is due to the elimination of graphite as moderator. For the thermal neutron we can see the flux depression around the guide tube. This flux depression is due to the absorption by SS-304 of the guide tube. The thermal neutron fluxes along the guide tube are about a factor of 2 smaller than those of case 1, whereas the absorption cross section of SS-304 is much larger than that of graphite. Then the introduction of the guide tube results in the formation of the strong gamma ray source region. In fact the gamma ray dose rate has a strong peak at the guide tube as can be seen in Fig.2.1.10.

It has already been known in the full reactor analysis that the neutrons and gamma rays leaked from the reactor vessel stream up through the cavity between the reactor vessel and the graphite shield, and then this streaming neutrons and gamma rays raise the flux levels in the voided region above the graphite shield. This is the reason why the flux level in the upper part of the guide tube penetration is not affected by the existence of the guide tube.

It becomes evident that the guide tube has effect of raising the secondary gamma ray dose rate, and that it has no significant effect on the neutron flux. We will see how much effective the case 2 model is on the comparison of the calculated results with measured values.

Table 2.1.1. Description of Regions in Case 1 and 2 Study

Region No.	Material	
	Case 1	Case 2
1	Graphite	Nitrogen
2	Graphite	SS-304
3	Graphite	Nitrogen
4	Graphite	Graphite
5	Nitrogen	Nitrogen
6	Nitrogen	SS-304
7	Nitrogen	Nitrogen
8	Fine flex*	Fine flex
9	Heavy concrete	Heavy Concrete

* Insulation

Table 2.1.2 Parameters Used in Cases 1 and 2 Calculation

Code	DOT 3.5
Quadrature	S - 120*
Scattering	P_3
Boundary conditions	Left : Reflective Right : Boundary source Bottom : Boundary source Top : Vacuum
Number of material zones	9
Number of mesh intervals	Radial : 11 Axial : 130
Number of energy groups	21 neutron & 7 gamma
General convergence criterion	0.01
Acceleration technique	Space dependent scaling
Flux calculation model	Weighted difference mode

* S-124 for Case 1 Calculation

Table 2.1.3 Energy group structure.

	No.	No.	Energy (ev)		Lethargy Width	Remarks
Neutron	1	1 - 10	1.4918+7	5.4881+6	1.0	
	2	11 - 15	5.4881+6		0.5	
	3	16 - 20	3.3287+6		0.5	
	4	21 - 25	2.0190+6		0.5	
	5	26 - 30	1.2246+6		0.5	
	6	31 - 35	7.4274+5		0.5	
	7	36 - 40	4.5049+5		0.5	
	8	41 - 45	2.7324+5		0.5	
	9	46 - 51	1.6573+5		0.9	
	10	52 - 55	6.7379+4		1.0	
	11	56 - 59	2.4788+4		1.0	
	12	60 - 63	9.1188+3		1.0	
	13	64 - 67	3.3546+3		1.0	
	14	68 - 71	1.2341+3		1.0	
	15	72 - 75	4.5400+2		1.0	
	16	76 - 80	1.6702+2		1.25	
	17	81 - 85	4.7851+1		1.25	
	18	86 - 90	1.3710+1		1.25	
	19	91 - 95	3.9279+0		1.25	
	20	96 - 99	1.1254+0		1.0	
	21	100	4.1399-1	1.0-3		
	No.	No.	Energy (MeV)		Energy Width	Remarks
Gamma	1	1 - 3	14.0	8.0	6.0	
	2	4 - 5	8.0		3.0	
	3	6 - 7	5.0		2.0	
	4	8 - 9	3.0		1.0	
	5	10 - 12	2.0		1.0	
	6	13 - 15	1.0		0.6	
	7	16 - 20	0.4	0.02	0.38	

Table 2.1.4 Description of S-120 Angle Quadrature (1/2)

ANGL	WEIGHT	ETA	MU
1	0.0	-0.9261810E+00	-0.3770792E+00
2	0.4403153E-01	-0.9261810E+00	-0.2666360E+00
3	0.4403153E-01	-0.9261810E+00	0.2666360E+00
4	0.0	-0.6815079E+00	-0.7318106E+00
5	0.3930152E-01	-0.6815079E+00	-0.6815079E+00
6	0.3930190E-01	-0.6815079E+00	-0.2666360E+00
7	0.3930190E-01	-0.6815079E+00	0.2666360E+00
8	0.3930152E-01	-0.6815079E+00	0.6815079E+00
9	0.0	-0.2666360E+00	-0.9637973E+00
10	0.4403153E-01	-0.2666360E+00	-0.9261810E+00
11	0.3930190E-01	-0.2666360E+00	-0.6815079E+00
12	0.4403162E-01	-0.2666360E+00	-0.2666360E+00
13	0.4403162E-01	-0.2666360E+00	0.2666360E+00
14	0.3930190E-01	-0.2666360E+00	0.6815079E+00
15	0.4403153E-01	-0.2666360E+00	0.9261810E+00
16	0.0	0.9998124E+00	-0.1936793E-01
17	0.4006299E-04	0.9998124E+00	-0.1870798E-01
18	0.4006299E-04	0.9998124E+00	-0.1369520E-01
19	0.4006299E-04	0.9998124E+00	-0.5012788E-02
20	0.4006299E-04	0.9998124E+00	0.5012788E-02
21	0.4006299E-04	0.9998124E+00	0.1369520E-01
22	0.4006299E-04	0.9998124E+00	0.1870798E-01
23	0.0	0.9990166E+00	-0.4433810E-01
24	0.9234800E-04	0.9990166E+00	-0.4282731E-01
25	0.9234800E-04	0.9990166E+00	-0.3135177E-01
26	0.9234800E-04	0.9990166E+00	-0.1147554E-01
27	0.9234800E-04	0.9990166E+00	0.1147554E-01
28	0.9234800E-04	0.9990166E+00	0.3135177E-01
29	0.9234800E-04	0.9990166E+00	0.4282731E-01
30	0.0	0.9976044E+00	-0.6917572E-01
31	0.1425480E-03	0.9976044E+00	-0.6681859E-01
32	0.1425480E-03	0.9976044E+00	-0.4891464E-01
33	0.1425480E-03	0.9976044E+00	-0.1790400E-01
34	0.1452480E-03	0.9976044E+00	0.1790400E-01
35	0.1425480E-03	0.9976044E+00	0.4891464E-01
36	0.1425480E-03	0.9976044E+00	0.6681859E-01
37	0.0	0.9956088E+00	-0.9361142E-01
38	0.1894150E-03	0.9956088E+00	-0.9042168E-01
39	0.1894150E-03	0.9956088E+00	-0.6619328E-01
40	0.1894150E-03	0.9956088E+00	-0.2422842E-01
41	0.1894150E-03	0.9956088E+00	0.2422842E-01
42	0.1894150E-03	0.9956088E+00	0.6619328E-01
43	0.1894150E-03	0.9956088E+00	0.9042168E-01
44	0.0	0.9930763E+00	-0.1174714E+00
45	0.2318420E-03	0.9930763E+00	-0.1134686E+00
46	0.2318420E-03	0.9930763E+00	-0.8306479E-01
47	0.2318420E-03	0.9930763E+00	-0.3040384E-01
48	0.2318420E-03	0.9930763E+00	0.3040384E-01
49	0.2318420E-03	0.9930763E+00	0.8306479E-01
50	0.2318420E-03	0.9930763E+00	0.1134686E-01
51	0.0	0.9900663E+00	-0.1406013E+00
52	0.2688360E-03	0.9900663E+00	-0.1358104E+00
53	0.2688360E-03	0.9900663E+00	-0.9942013E-01
54	0.2688360E-03	0.9900663E+00	-0.3639031E-01
55	0.2688360E-03	0.9900663E+00	0.3639031E-01
56	0.2688360E-03	0.9900663E+00	0.9942013E-01
57	0.2688360E-03	0.9900663E+00	0.1358104E+00
58	0.0	0.9866495E+00	-0.1628584E+00
59	0.2995280E-03	0.9866495E+00	-0.1573091E+00

Table 2.1.4 (Continued) (2/2)

ANGL	WEIGHT	ETA	MU
60	0.2995280E-03	0.9866495E+00	-0.1151583E+00
61	0.2995280E-03	0.9866495E+00	-0.4215085E-01
62	0.2995280E-03	0.9866495E+00	0.4215085E-01
63	0.2995280E-03	0.9866495E+00	0.1151583E+00
64	0.2995280E-03	0.9866495E+00	0.1573091E+00
65	0.0	0.9829057E+00	-0.1841094E+00
66	0.3232011E-03	0.9829057E+00	-0.1778361E+00
67	0.3232011E-03	0.9829057E+00	-0.1301850E+00
68	0.3232011E-03	0.9829057E+00	-0.4765103E-01
69	0.3232011E-03	0.9829057E+00	0.4765103E-01
70	0.3232011E-03	0.9829057E+00	0.1301850E+00
71	0.3232011E-03	0.9829057E+00	0.1778361E+00
72	0.0	0.9789229E+00	-0.2042298E+00
73	0.3392971E-03	0.9789229E+00	-0.1972709E+00
74	0.3392971E-03	0.9789229E+00	-0.1444123E+00
75	0.3392971E-03	0.9789229E+00	-0.5285857E-01
76	0.3392971E-03	0.9789229E+00	0.5285857E-01
77	0.3392971E-03	0.9789229E+00	0.1444123E+00
78	0.3392971E-03	0.9789229E+00	0.1972709E+00
79	0.0	0.9747944E+00	-0.2231048E+00
80	0.3474411E-03	0.9747944E+00	-0.2155027E+00
81	0.3474411E-03	0.9747944E+00	-0.1577590E+00
82	0.3474411E-03	0.9747944E+00	-0.5774379E-01
83	0.3474411E-03	0.9747944E+00	0.5774379E-01
84	0.3474411E-03	0.9747944E+00	0.1577590E+00
85	0.3474411E-03	0.9747944E+00	0.2155027E+00
86	0.0	0.9492823E+00	-0.3144249E+00
87	0.3903883E-02	0.9492823E+00	-0.3037111E+00
88	0.3903883E-02	0.9492823E+00	-0.2223319E+00
89	0.3903883E-02	0.9492823E+00	-0.8137912E-01
90	0.3903883E-02	0.9492823E+00	0.8137912E-01
91	0.3903883E-02	0.9492823E+00	0.2223319E+00
92	0.3903883E-02	0.9492823E+00	0.3037111E+00
93	0.0	0.9024357E+00	-0.4308245E+00
94	0.3903903E-02	0.9024357E+00	-0.4161445E+00
95	0.3903903E-02	0.9024357E+00	-0.3046389E+00
96	0.3903903E-02	0.9024357E+00	-0.1115056E+00
97	0.3903903E-02	0.9024357E+00	0.1115056E+00
98	0.3903903E-02	0.9024357E+00	0.3046389E+00
99	0.3903903E-02	0.9024357E+00	0.4161445E+00
100	0.0	0.7867957E+00	-0.6172134E+00
101	0.2268518E-01	0.7867957E+00	-0.5773503E+00
102	0.2268518E-01	0.7867957E+00	-0.2182178E+00
103	0.2268518E-01	0.7867957E+00	0.2182178E+00
104	0.2268518E-01	0.7867957E+00	0.5773503E+00
105	0.0	0.5773503E+00	-0.8164966E+00
106	0.2268518E-01	0.5773503E+00	-0.7867957E+00
107	0.2314814E-01	0.5773503E+00	-0.5773503E+00
108	0.2268518E-01	0.5773503E+00	-0.2182178E+00
109	0.2268518E-01	0.5773503E+00	0.2182178E+00
110	0.2314814E-01	0.5773503E+00	0.5773503E+00
111	0.2268518E-01	0.5773503E+00	0.7867957E+00
112	0.0	0.2182178E+00	-0.9759001E+00
113	0.3024691E-01	0.2182178E+00	-0.9511897E+00
114	0.2268518E-01	0.2172178E+00	-0.7867957E+00
115	0.2268518E-01	0.2182178E+00	-0.5773503E+00
116	0.3024691E-01	0.2182178E+00	-0.2182178E+00
117	0.3024691E-01	0.2182178E+00	0.2182178E+00
118	0.2268518E-01	0.2182178E+00	0.5773503E+00
119	0.2268518E-01	0.2182178E+00	0.7867957E+00
120	0.3024691E-01	0.2182178E+00	0.9511897E+00

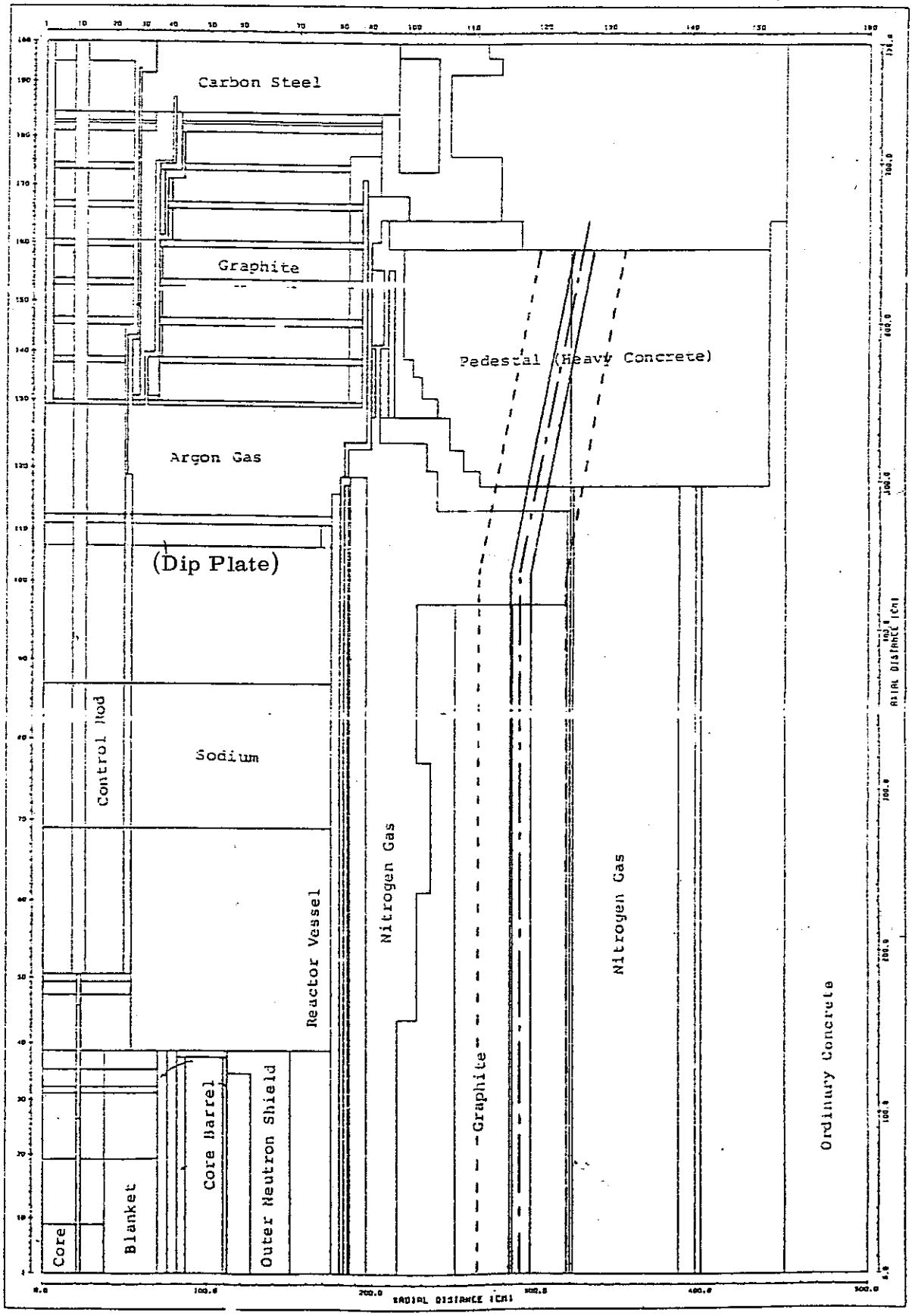

Fig. 2.1.1 Calculational Region in This Study Relative to Full Reactor Shielding Analysis

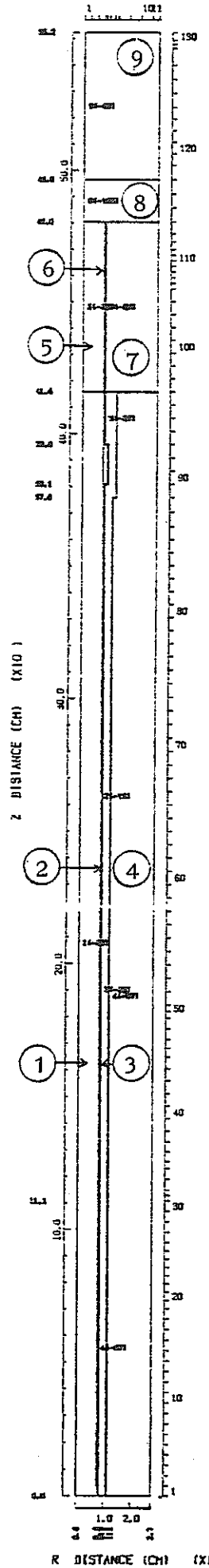

Fig.2.1.2 Calculational Geometry for analysis of the effect of the guide tube. Refer to Table 2.1.1. for region identification

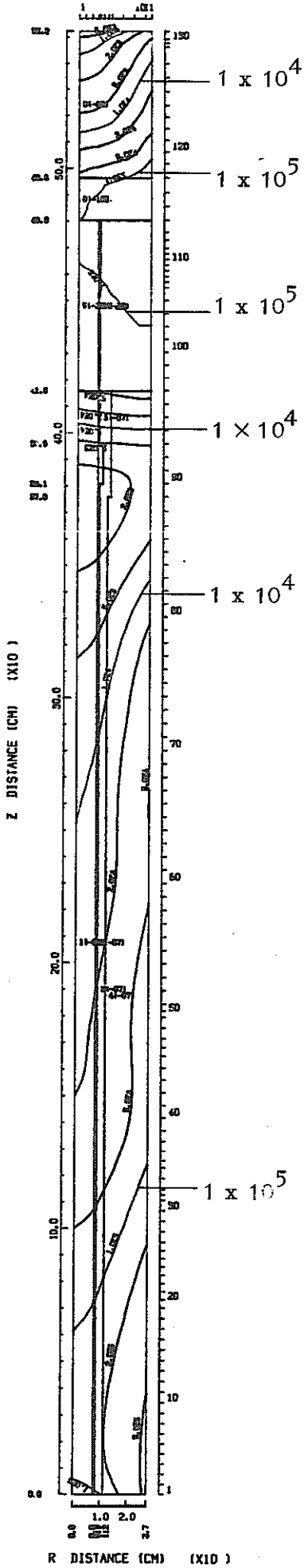

Fig. 2.1.3 Isoflux Contours for Case 1 Study

FAST NEUTRON FLUX (N/CM**2.S) 1.4918E+07 - 7.4274E+05 (EV) (GROUP 1-5)

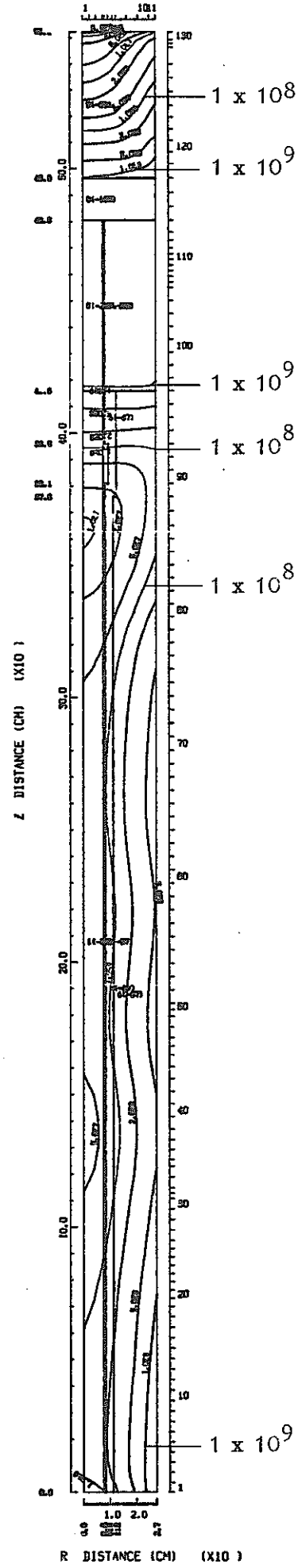

Fig.2.1.4 Isoflux Contours for Case 1 Study

INTERMEDIATE NEUTRON FLUX (N/CM**2.S) 7.4274E+05 - 4.1399E-01 (EV) (GROUP 6-20)

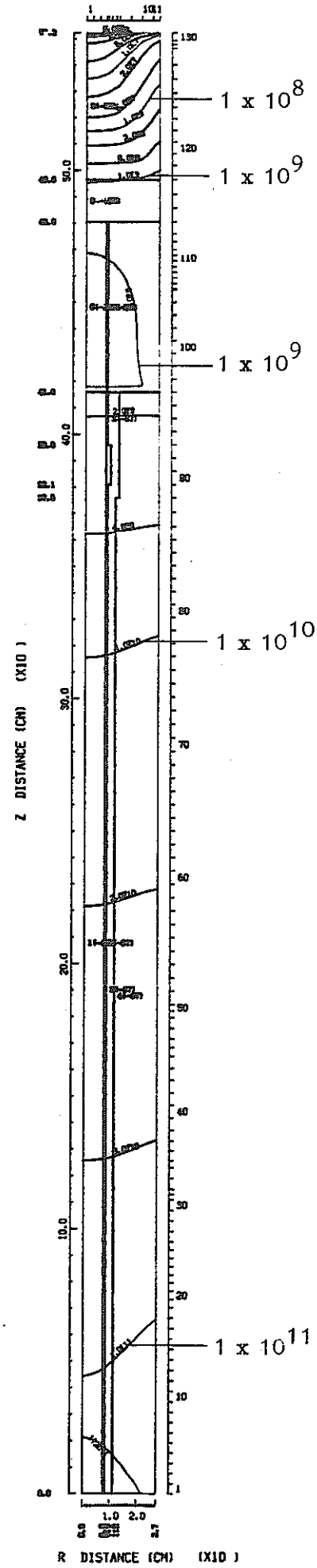

Fig.2.1.5 Isoflux Contours for Case 1 Study

THERMAL NEUTRON FLUX (N/CM**2.S) 4.1399E-01 - 1.0000E-03 (EV) (GROUP 21-21)

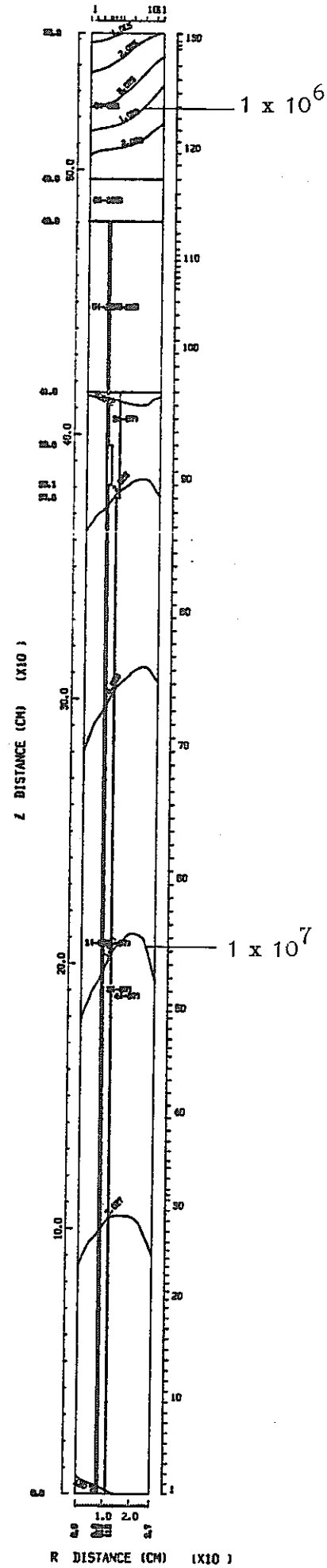

Fig.2.1.6 Isodose-rate Contours for Case 1 Study

GAMMA DOSE RATE (MREM/HOUR) 1.4000E+07 - 2.0000E+04 (EV) (GROUP 22-28)

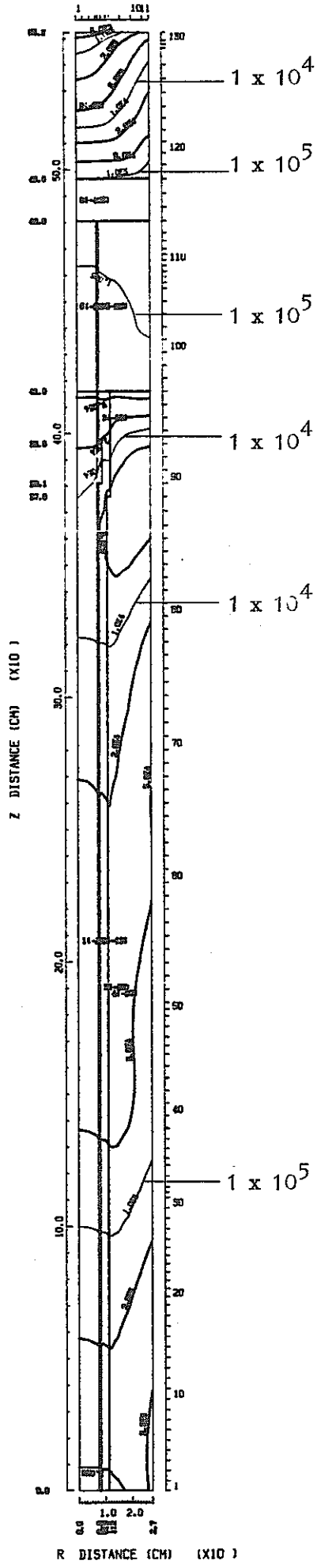

Fig.2.1.7 Isoflux Contours for Case 2 Study

FAST NEUTRON FLUX (N/CM**2.S) 1.4918E+07 - 7.4274E+05 (EV) (GROUP 1-5)

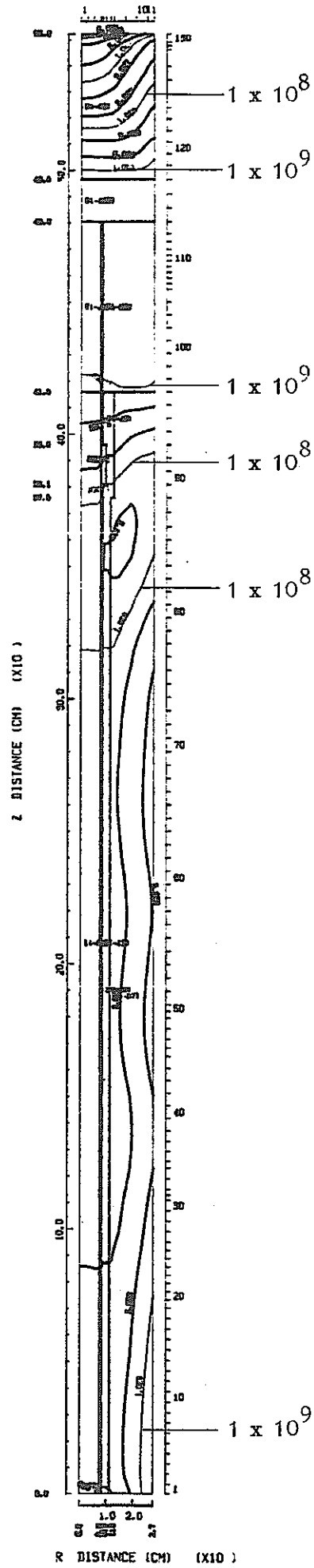

Fig.2.1.8 Isolfux Contours for Case 2 Study

INTERMEDIATE NEUTRON FLUX (N/CM**2.S) 7.4274E+05 - 4.1399E-01 (EV) (GROUP 6-20)

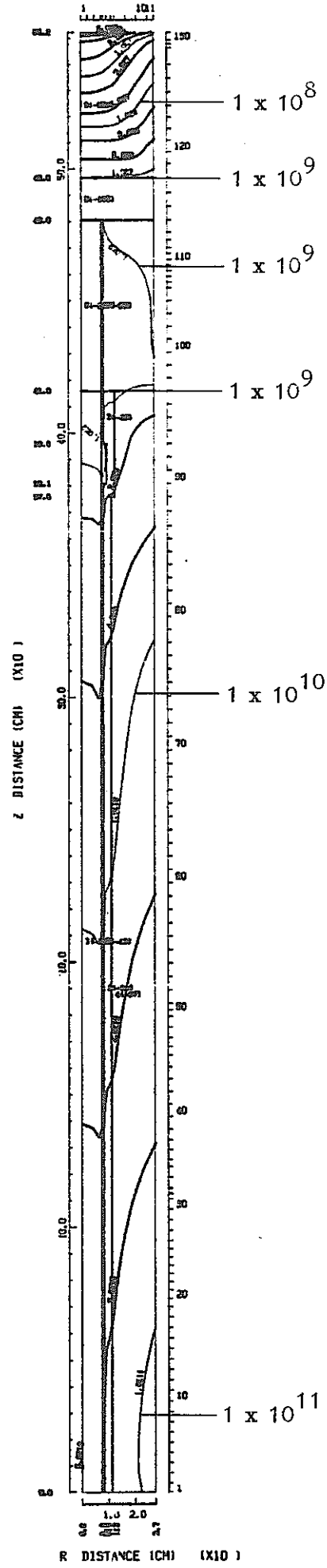

Fig.2.1.9 Isoflux Contours for Case 2 Study

THERMAL NEUTRON FLUX (N/CM**2.S) 4.1399E-01 - 1.0000E-03 (EV) (GROUP 21-21)

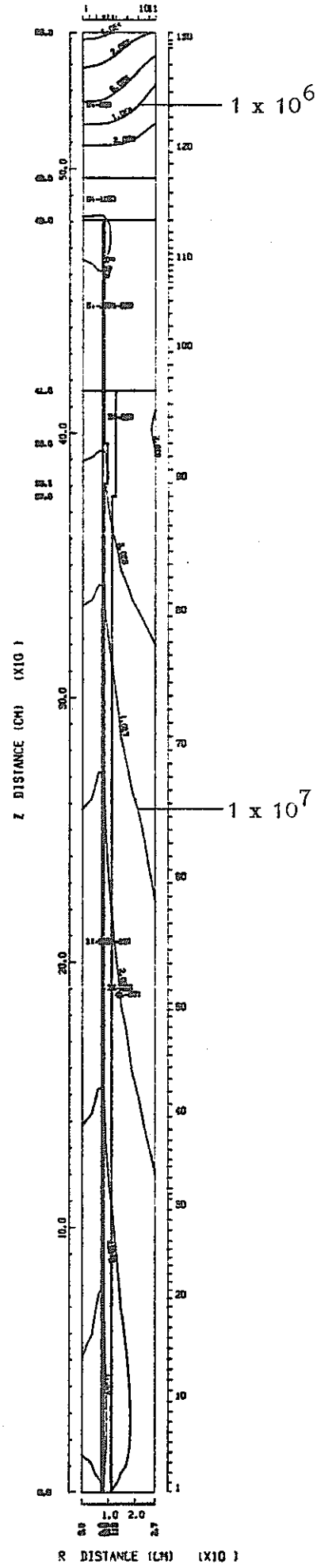

Fig.2.1.10 Isodose-rate Contours for Case 2 Study

GAMMA DOSE RATE (MREM/HOUR) 1.4000E+07 - 2.0000E+04 (EV) (GROUP 22-28)

2.2 Detector guide tube penetration in the heavy concrete pedestal

When the calculated thermal neutron flux obtained by the full reactor analysis was compared with that measured along the detector guide tube penetration of channel A in the heavy concrete pedestal, the calculated flux was a factor of 5.6×10^{-3} smaller than the measured flux at the exit of the penetration (at the top surface of the pedestal), while it was higher by a factor of about 3 than the measured one at the entrance of the penetration. For gamma dose rates, the calculated to measured dose rate ratio was 0.14 at a level 600 cm from the core mid-plane (this level locates at point about 100 cm from the entrance of penetration of which length is about 150 cm) and 0.45 or 1.29 at the entrance depending on the detector used. In the full reactor shielding analysis, we did not take into account any effects of the guide tube penetration. It was easily anticipated that the streaming effect of the penetration enhances the neutron and gamma ray flux level.

In this section we will discuss about the analysis of the streaming by our shielding method developed in the previous section. Unfortunately, however, the guide tube penetrates the heavy concrete pedestal with 10 deg obliquity. Therefore we had to adjust the angular flux of the source for streaming analysis.

2.2.1 Calculational model

The geometry used in this calculation is shown in Fig. 2.2.1 with the regions identified in Table 2.2.1. The center axis of this R-Z geometry corresponds to that of the guide tube. Considering the obliquity of the penetration the region extends from a level of 430 cm from the core mid-plane to the nitrogen space above the pedestal. The top surface of the pedestal is 656 cm in the model, while actual level is 646 cm from the core mid-plane.

The boundary angular flux on the bottom boundary was obtained from the results of previous graphite shield penetration calculation. In order to take into account the 10 deg obliquity of the bottom plane, the incoming angular flux was determined by the similar method to the angular flux adjustment between different number quadrature sets. There are two selections to define the boundary angular flux at the bottom boundary due to the rotational symmetry of the two dimensional cylindrical geometry.

The boundary angular flux on the right boundary was obtained from the results of Step 4 calculation in the full reactor shielding analysis. Again we needed to adjust the incoming flux adequate to the obliquity of the pedestal. In this case we needed to select the special mesh in the previous analysis that corresponds to the new special mesh. Table 2.2.2 summarizes the calculational parameters used in this penetration analysis.

2.2.2 Calculational results

The neutron flux and gamma ray dose rate contours from this calculation are shown in Figs. 2.2.2 through 2.2.5. In these figures, contours are for 1.0×, 2.0× and 5.0×10^{n}. The neutron fluxes at the exit of the penetration are about 5×10^{1}, 7×10^{5} and 7×10^{5} n/cm^{2}·s, respectively for the fast, intermediate and thermal neutrons, while in the full reactor analysis, they were about 10^{0}, 10^{4} and 10^{3} n/cm^{2}·s. Since the flux levels at the entrance of the penetration are almost the same for these two analysis, it can be seen that the guide tube penetration has a streaming effect that enhances the neutron flux at the exit about a factor of 50 to 700.

For the gamma ray, the dose rate at the exit is about 10^{4} mrem/h, while that was about 2×10^{2} mrem/h in the full reactor analysis. It can be conceivable that there are two sources that enhance the gamma dose

rates; one is the streaming effect and the other is the increasement of the secondary gamma ray source at the guide tube due to the increasement of the neutron flux. Though it is not evaluated quantitatively which is dominant, the streaming effect might be larger than the effect of the increased secondary gamma ray source by considering there is no evident peak in the gamma ray dose rate at the guide tube.

As to the boundary angular flux adjustments at the bottom plane, there was no significant difference between two types of the adjustment. This is attributed to the fact that the obliquity is small.

Table 2.2.1 Description of Regions for Streaming Analysis

Region No.	Material
1	Nitrogen
2	SS - 304
3	Nitrogen
4	Nitrogen
5	SS - 304
6	Fine flex
7	Nitrogen
8	SS - 304
9	Heavy concrete
10	SS - 304
11	Nitrogen
12	SS - 304
13	Nitrogen

Table 2.2.2 Parameters Used for Streaming Analysis

Code	DOT 3.5
Quadrature	S - 120
Scattering	P_3
Boundary conditions	Left : Reflective
	Right : Boundary flux
	Bottom : Boundary flux
	Top : Vacuum
Number of material zones	13
Number of mesh intervals	Radial : 11
	Axial : 77
Number of energy groups	21 neutron & 7 gamma
General convergence criterion	0.01
Acceleration technique	Space dependent scaling
Flux calculation model	Weighted difference mode

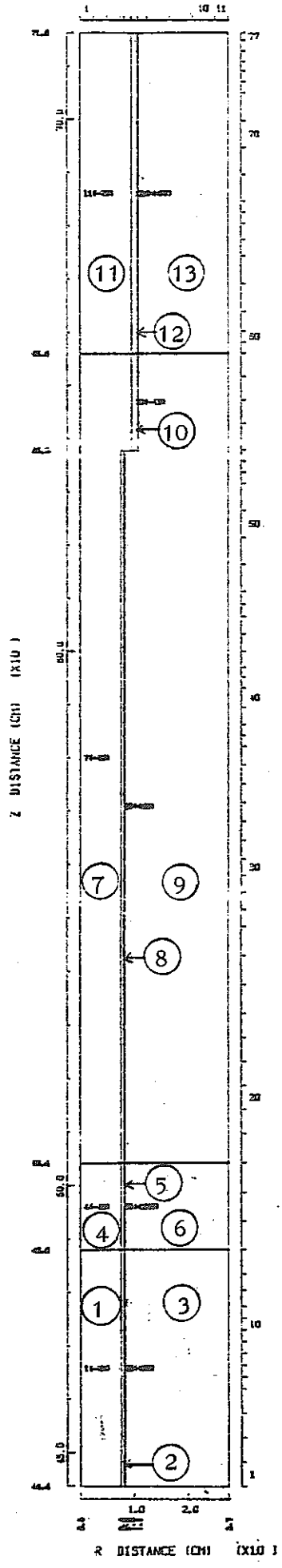

Fig.2.2.1 Calculational Geometry for Streaming Analysis

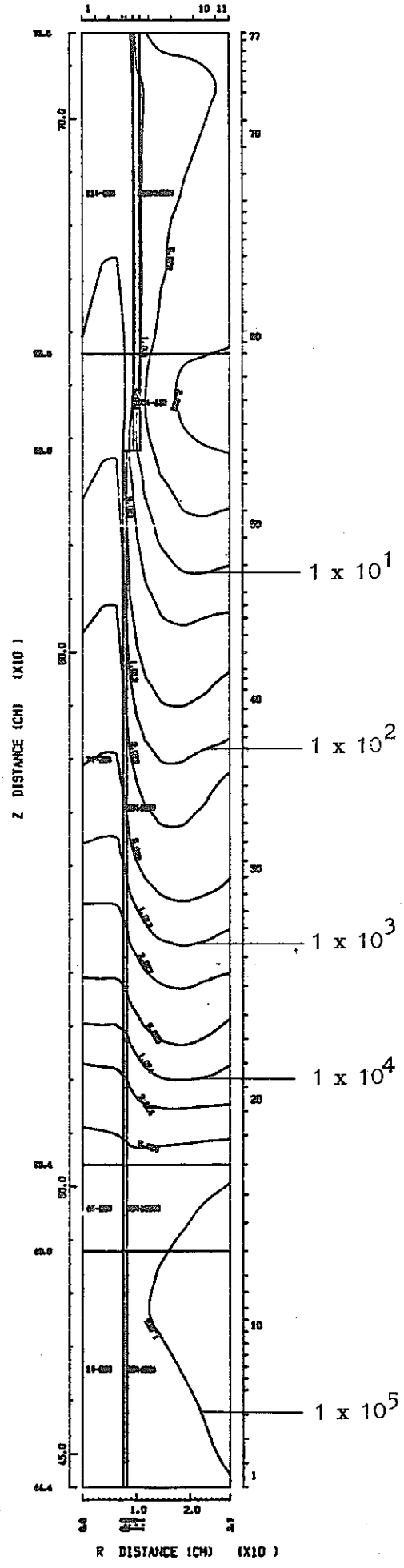

Fig.2.2.2 Isoflux Contours for Streaming Analysis

FAST NEUTRON FLUX (N/CM**2.S) 1.4918E+07 - 7.4274E+05 (EV) (GROUP 1-5)

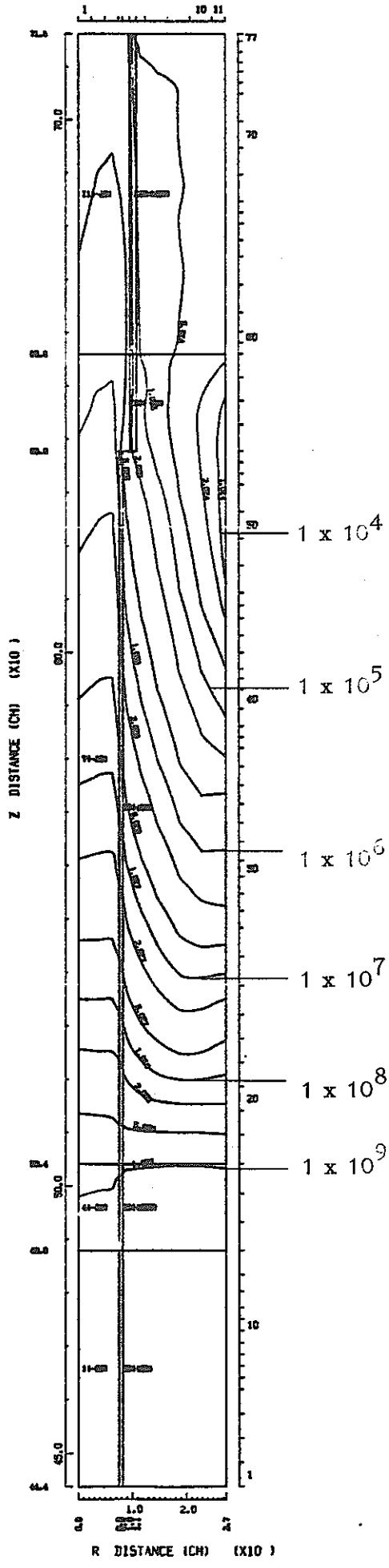

Fig.2.2.3 Isoflux Contours for Streaming Analysis.

INTERMEDIATE NEUTRON FLUX (N/CM**2.S) 7.4274E+05 - 4.1399E-01 (EV) (GROUP 6-20)

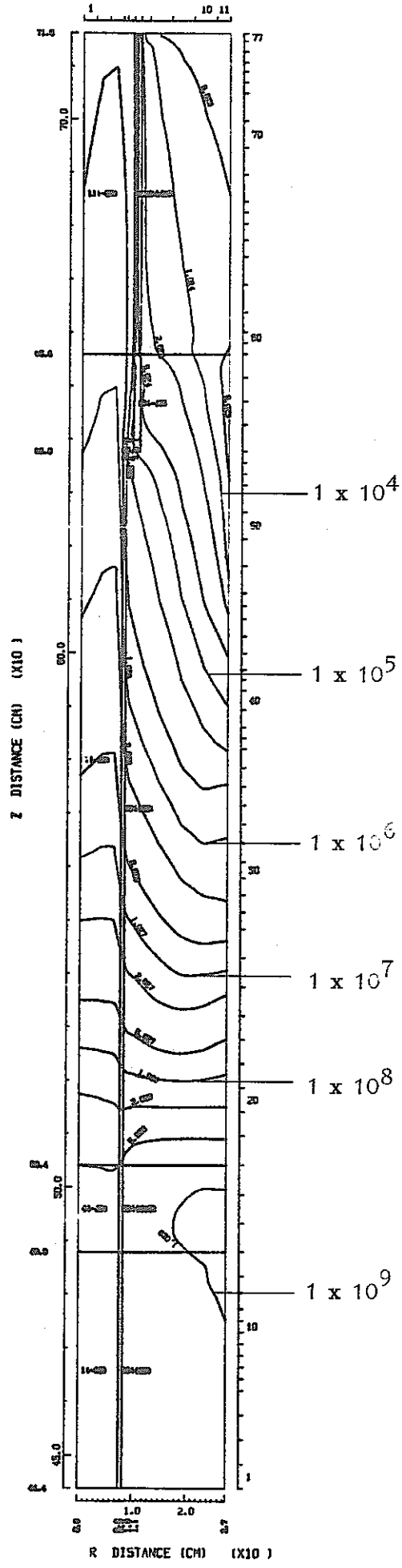

Fig.2.2.4 Isoflux Contours for Streaming Analysis

THERMAL NEUTRON FLUX (N/CM**2.S) 4.1399E-01 - 1.0000E-03 (EV) (GROUP 21-21)

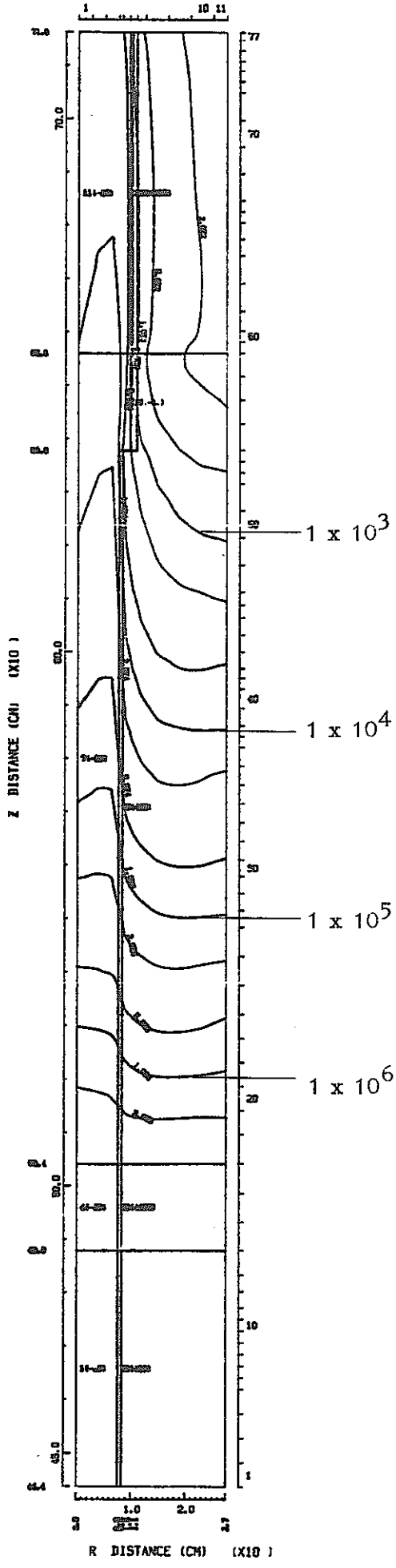

Fig. 2.2.5 Isodose-rate Contours for Streaming Analysis

GAMMA DOSE RATE (MREM/HOUR) 1.4000E+07 - 2.0000E+04 (EV) (GROUP 22-28)

2.3 Comparison of calculated results with measured results

2.3.1 Gamma ray dose rates in detector guide tube

The calculated gamma ray dose rates along the detector guide tube are shown in Table 2.3.1 in comparison with the measured dose rates and the calculated dose rates by the full reactor shielding analysis. The height of the graphite shield is 416 cm and the pedestal occupies heights from 500 cm to 646 cm. The calculated dose rates corresponding to heights from 0 cm to 430 cm are obtained from the case 1 study and the other dose rates from the case 2 study. It can be seen that there is a difference of a factor of about 15 between the results with and without considering the secondary gamma rays due to the guide tube. The calculational to experimental values were in the range of 0.03 to 0.09 in the full reactor analysis. They are improved to the range of 0.32 to 1.08.

In the penetration in the pedestal, an attenuation factor of the gamma dose rate from H=500 cm to 600 cm is 5×10^{-3} for the measurement. The streaming analysis of the case 2 study gives a factor of 8.8×10^{-3} that agrees well with the measured value.

2.3.2 Thermal neutron flux in detector guide tube

The calculated thermal fluxes along the detector guide tube are shown in Table 2.3.2 in comparison with the measured thermal fluxes. As has been proved in the previous section the thermal flux in the region of graphite shield are not affected by the detector guide tube. The primary interest is the thermal flux along the guide tube in the concrete pedestal which correspond to the data in columns of H=500, 550, 600 and 650 cm in Table 2.3.2. From these data we can see the streaming analysis of this study well agree with the measured results. For example,

the attenuation factor of the thermal neutron flux from H=500 cm to 600 cm is 5.13×10^{-3} by the $^{10}B(n, \alpha)$ reaction measurement and 3.33×10^{-3} by gold foil measurement, while the calculated attenuation is 4.62×10^{-3}. The attenuation from H=500 cm to 650 cm is 7.16×10^{-4} by $^{10}B(n, \alpha)$ reaction measurement and 1.75×10^{-3} by calculation.

The calculational to experimental value of the thermal neutron flux at the exit of the penetration is improved from 5.6×10^{-3} by the full reactor analysis to 8.0 by the streaming analysis in this study.

Table 2.3.1 Comparison of the Calculated Gamma Ray Dose Rate with Measurement

Height (cm)	Calculated		γ-IC Measurement			TLD Measurement		
			Measured	C/E		Measured	C/E	
	Present	Full reactor		Present	Full reactor		Present	Full reactor
0	7.08+7	7.80+6	-	-	-	2.20+8	0.32	0.035
10	9.42+7	7.79+6	1.50+8	0.63	0.052	-	-	-
25	1.08+8	7.28+7	-	-	-	2.16+8	0.50	0.034
40	1.06+8	6.65+6	1.32+8	0.80	0.050	-	-	-
50	1.03+8	6.37+6	-	-	-	1.89+8	0.54	0.034
70	9.24+7	5.71+6	1.09+8	0.86	0.053	-	-	-
100	7.17+7	4.56+6	9.13+7	0.78	0.050	1.23+8	0.58	0.037
130	5.41+7	3.59+6	6.73+7	0.80	0.053	-	-	-
150	4.64+7	3.23+6	-	-	-	6.74+7	0.69	0.048
160	4.27+7	3.01+6	4.70+7	0.91	0.064	-	-	-
190	3.26+7	2.48+6	3.58+7	0.91	0.069	-	-	-
200	2.99+7	2.32+6	-	-	-	3.97+7	0.75	0.058
220	2.56+7	2.07+6	2.74+7	0.94	0.075	-	-	-
250	2.10+7	1.74+6	2.17+7	0.97	0.080	-	-	-
280	1.75+7	1.47+6	1.40+7	1.25	0.11	-	-	-
300	1.50+7	1.26+6	-	-	-	1.39+7	1.08	0.091
310	1.37+7	1.14+6	9.04+6	1.51	0.13	-	-	-
340	9.67+6	8.05+5	6.56+6	1.47	0.12	-	-	-
370	6.39+6	5.69+5	5.31+6	1.20	0.11	-	-	-
400	4.29+6	5.29+5	5.04+6	0.85	0.10	6.74+6	0.64	0.078
430	2.69+6	1.21+6	5.63+6	0.48	0.21	-	-	-
460	4.47+6	1.53+6	4.66+6	0.96	0.33	-	-	-
490	4.01+6	1.83+6	1.38+6	2.82	1.29	-	-	-
500	3.31+6	1.56+6	-	-	-	3.44+6	0.96	0.45
600	2.91+4	2.34+3	-	-	-	1.72+4	1.69	0.14

Table 2.3.2 Comparison of the Calculated Thermal Neutron Flux with Measurement

H[1] (cm)	Calculated flux		Measured flux			C/E[5]					
	Full reactor	Present	E1[2]	E2[3]	E3[4]	E1		E2		E3	
0.0	4.49+10	4.97+10	2.12+10	-	2.12+10	2.12	2.34	-	-	2.12	2.34
25.0	3.40+10	4.90+10	-	-	2.24+10	-	-	-	-	1.52	2.19
50.0	2.63+10	4.49+10	1.78+10	-	2.03+10	1.48	2.52	-	-	1.30	2.21
75.0	2.45+10	3.79+10	-	1.62+10	-	-	-	1.51	2.34	-	-
100.0	1.96+10	3.00+10	1.18+10	-	1.14+10	1.66	2.54	-	-	1.72	2.63
150.0	1.22+10	1.80+10	6.75+9	7.17+9	8.88+9	1.80	2.67	1.70	2.50	1.37	2.03
200.0	8.17+9	1.09+10	4.48+9	4.41+9	5.35+9	1.82	2.44	1.85	2.48	1.53	2.04
250.0	6.03+9	7.23+9	2.97+9	2.96+9	-	2.03	2.43	2.04	2.44	-	-
300.0	4.55+9	5.33+9	1.66+9	1.62+9	1.39+9	2.75	3.21	2.81	3.29	3.28	3.84
350.0	2.01+9	2.91+9	7.83+8	7.13+8	-	2.56	3.72	2.82	4.08	-	-
400.0	1.17+9	9.64+8	3.42+8	5.54+8	3.97+8	3.41	2.82	2.11	1.74	2.97	2.43
450.0	5.92+8	6.28+8	2.72+8	2.36+8	-	2.17	2.31	2.51	2.66	-	-
500.0	4.13+8	4.24+8	1.29+8	8.72+8	1.68+8	3.19	3.27	0.47	0.49	2.45	2.53
550.0	7.44+5	1.15+7	4.94+6	-	-	0.15	2.94	-	-	-	-
600.0	1.96+4	1.96+6	6.64+5	-	5.60+5	0.029	2.96	-	-	0.035	3.51
650.0	5.13+2	7.42+5	9.23+4	-	-	5.6-3	8.03	-	-	-	-

1) Height from the core mid-plane

2) Thermal neutron flux obtained from $^{10}B(n, \alpha)$ reaction measurement

3) " gold foil "

4) " thermoluminescence detector

5) C/E for the above three measured data; Left side is for the full reactor calculation and right side is for the present analysis.

2.4 Simple analytical method for the effect of the detector guide tube penetration

Of frequently significant use in the reactor shielding design is the simple analytical approximation particularly to the perturbation introduced by the geometrical irregurality. We will attempt in this section the application of the simple analytical method and compare the result with the measured values.

Simple analytical approach to the investigation of the effect of the detector guide tube is, as in the analysis by the discrete ordinates code, devided into two parts, one is for the penetration in the graphite shield and the other for the penetration in the heavy concrete shield. Simple analysis is generally applied to evaluate perturbation effects introduced in a uniform shield by geometrical irregularities. Then we assume that the neutron and gamma ray fluxes are known in the uniform shield geometry.

2.4.1 Guide tube in the graphite shield

It has been known from the full reactor shielding analysis that the neutron flux attenuation in the graphite shield was pronounced in the radial direction and almost uniform in the axial direction. It can be anticipated that the neutron flux will not be significantly affected by the introduction of the irregularity which lies in the axial direction, since this irregurality is primarily composed of voids. It can also be anticipated that the guide tube introduces perturbation of the gamma ray flux due to the secondary gamma ray emitted from a thin guide tube material.

We use the following assumptions to make ease an evaluation of the secondary gamma ray dose rate around the guide tube.

1. Secondary gamma ray production by the fast and intermediate neutrons is neglegiblly small.

2. Thermal neutron flux distribution is piece-wise constant along the axial direction and uniform in the radial direction.

3. Gamma ray absorption of the guide tube can be neglected.

All these assumptions are seemed valid considering the neutron energy spectrum, gamma ray production cross section of SS-304 and a thickness of 0.7 cm of the guide tube.

We devide, along the axial direction, the guide tube into I regions, $[H_L^i, H_U^i]$ for i = 1, 2, ..., I, in which the thermal flux is constant. The gamma ray dose rate D on the center axis of the guide tube can be evaluated by the following equation.

$$D = \frac{\triangle R}{2} \sum_g \sum_i K_g S_g^i \left[\tan^{-1} \frac{H_U^i - H}{R} - \tan^{-1} \frac{H_L^i - H}{R} \right], \quad \ldots. \quad (2.4.1)$$

where

R : inner radius of the guide tube

$\triangle R$: thickness of the guide tube

H : height of dose rate calculation point

K_g : flux to dose rate conversion factor

S_g^i : gamma ray source of energy group g, where g's are from 22 to 28 corresponding our coupled neutron and gamma ray energy group structure

$$S_g^i = \Sigma_{21 \to g} \phi_{21}^i \quad (2.4.2)$$

$\Sigma_{21 \to g}$: gamma ray production cross section of thermal neutron for SS-304

ϕ_{21}^i : thermal neutron flux in region i

In the numerical calculation we use the piece-wise constant flux distribution along the axial direction as shown in Fig. 2.4.1. The secondary gamma ray production cross section of SS-304 due to the thermal neutron capture is the same data as those used in the full reactor analysis and shown in Table 2.4.1, where the data for the graphite and the gamma ray flux to dose rate conversion factor are also shown. In the simple analysis the average gamma ray energy was used as shown in this table.

The numerical results are shown in Table 2.4.2 in comparison with the results by the discrete ordinates code and the measured dose rates. It can be seen that the simple analysis gives almost the same results as those by the discrete ordinates code.

2.4.2 Guide tube in the heavy concrete pedestal

It is evident that the effect of the guide tube penetration on the neutron and gamma ray fluxes is the streaming through the penetration in the pedestal. We will evaluate a direct streaming flux and a single scattering flux by the penetration wall using the simple method generally applied in the reactor shielding design.

For direct streaming fluxes we use the equation given by

$$\phi_{ex} = \frac{n+1}{2} \phi_{en} \frac{R^2}{L^2} \quad , \qquad (2.4.3)$$

where we assumed the usual μ^n - angular distribution of the source, and

ϕ_{ex} : flux at exit

ϕ_{en} : flux at entrance

R : inner radius of penetration

L : length of penetration

For single scattering fluxes we use the Simon - Clifford equation modified to the multigroup treatment. Using the same method as developed

in the original Simon-Clifford equation we can obtain the expression for the single scattering flux at the exit as

$$\phi_{ex}^{g} = \frac{\pi R^3}{8L^3} \sum_{g'} \phi_{en}^{g'} \sigma_{g' \to g}^{s} \left[\frac{1}{\sigma_{g'}} + \frac{1}{\sigma_{g}} \right] , \quad (2.4.4)$$

where

ϕ_{ex}^{g} : flux of energy group g at exit

$\phi_{en}^{g'}$: flux of energy group g' at entrance

$\sigma_{g' \to g}^{s}$: transfer cross section of penetration wall material from the energy group g' to g

σ_{g} : total cross section of penetration wall material of energy group g.

By using the total upwards flux at the entrance of the penetration obtained from the case 2 study of Section 2.1 the flux at exit can be calculated as shown in Table 2.4.3,where we assumed the source fluxes are isotropic (n=0 in Eq.(2.4.3)). These results are compared with those by the discrete ordinates method. It can be seen from this table that the fast fluxes at exit are smaller than those by DOT 3.5, the intermediate fluxes are comparable to the results by DOT3.5 and the thermal flux (group 21) and gamma fluxes (groups 22 - 28) are smaller than those by DOT3.5. The reason is attributed to the fact that the angular flux distribution at entrance is highly peaked to upwards except the intermediate neutron fluxes. In Figs. 2.4.2 to 2.4.4 the angular flux distributions on (μ, η) plane with $\mu < 0$ are shown, where μ and η are direction ordinates of usual meaning. The angular fluxes have their peak towards $\eta \approx 0.985$ direction due to the oblique penetration. If we neglect the obliquity of the penetration and apply the μ^n distribution in the meaning of Eq.(2.4.3), it will lead to a great overestimation. Therefore, the simple analytical method fails in these situations and in order to estimate the streaming fluxes a fairly exact angular distribution has to be taken into account in deriving the equation corresponding to Eq. (2.4.3).

Table 2.4.1 Secondary Gamma Ray Production Corss Section for SS-304 and Graphite

Group	Energy Range (MeV)	Average Energy (MeV)	Cross Section (cm^{-1})		Flux to Dose Rate Conversion Factor*
			SS-304	Graphite	
22	14 - 8	10	4.983 - 2	1.178 - 6	1.071 - 1
23	8 - 5	6.5	9.299 - 2	4.046 - 6	7.612 - 2
24	5 - 3	4.0	3.265 - 2	1.877 - 4	5.332 - 2
25	3 - 2	2.5	2.763 - 2	6.342 - 7	3.840 - 2
26	2 - 1	1.5	4.405 - 2	5.742 - 5	2.652 - 2
27	1 - 0.4	0.7	2.618 - 2	2.623 - 4	1.410 - 2
28	0.4 - 0.02	0.2	7.853 - 2	0.0	1.012 - 2

* Unit is $[\,^{mrem}/_{h}\,] \;/\; [\;\gamma/cm^2.S\;]$

Table 2.4.2 Gamma Ray Dose Rate along the Detector Tube in Graphite Shield

Distance from Core Mid-Plane (cm)	Dose Rate (mrem/h)				C/E	
	γ-IC	TLD-700	Simple	DOT3.5	Simple	DOT3.5
-100	-	1.03+8	4.29+7	-	0.42	-
- 90	8.09+7	-	6.60+7	-	0.82	-
- 60	1.03+8	-	9.14+7	-	0.89	-
- 50	-	1.70+8	9.68+7	-	0.57	-
- 20	1.42+8	-	1.05+8	-	0.74	-
- 0	-	2.20+8	1.04+8	7.08+7	0.47	0.32
10	1.50+8	-	1.05+8	9.42+7	0.70	0.63
25	-	2.16+8	1.05+8	1.08+8	0.49	0.50
40	1.32+8	-	1.02+8	1.06+8	0.77	0.80
50	-	1.89+8	9.82+7	1.03+8	0.52	0.54
70	1.09+8	-	8.83+7	9.24+7	0.81	0.86
100	9.13+7	1.23+8	6.98+7	7.17+7	0.76	0.58
130	6.73+7	-	5.25+7	5.41+7	0.78	0.80
150	-	6.74+7	4.32+7	4.64+7	0.64	0.69
160	4.70+7	-	3.94+7	4.27+7	0.84	0.91
190	3.58+7	-	3.04+7	3.26+7	0.85	0.91
200	-	3.97+7	2.79+7	2.99+7	0.70	0.75
220	2.74+7	-	2.36+7	2.56+7	0.86	0.94
250	2.17+7	-	1.89+7	2.10+7	0.87	0.97
280	1.40+7	-	1.54+7	1.75+7	1.1	1.25
300	-	1.39+7	1.33+7	1.50+7	0.96	1.08
310	9.05+6	-	1.21+7	1.37+7	1.34	1.51
340	6.56+6	-	8.60+6	9.67+6	1.31	1.47
370	5.31+6	-	5.66+6	6.39+6	1.07	1.20
400	5.04+6	6.74+6	3.65+6	4.29+6	0.72	0.64
430	5.63+6	-	2.14+6	2.69+6	0.38	0.48
460	4.66+6	-	1.82+6	4.47+6	0.39	0.96
490	1.38+6	-	1.43+6	4.01+6	1.04	2.82
500	-	3.44+6	9.90+5	3.31+6	0.29	0.96

γ-IC and TLD-700 are detectors.

Simple means dose rates calculated by simple analytical method.

Table 2.4.3 Streaming Flux by Simple Analytical Method

Group*	Flux at Exit Simple	DOT3.5	Simple/DOT3.5
1	6.59-2	2.38-1	0.28
2	1.50-1	4.25-1	0.35
3	7.77-1	1.72+0	0.45
4	6.49+0	9.35+0	0.69
5	3.70+1	4.72+1	0.78
6	1.13+2	1.77+2	0.64
7	4.63+2	6.48+2	0.71
8	1.27+3	1.53+3	0.83
9	7.05+3	8.89+3	0.79
10	1.75+4	1.97+4	0.89
11	2.48+4	2.26+4	1.10
12	3.42+4	2.95+4	1.16
13	3.86+4	3.34+4	1.15
14	4.79+4	4.33+4	1.11
15	5.60+4	4.98+4	1.12
16	8.65+4	7.94+4	1.09
17	1.25+5	1.15+5	1.09
18	1.51+5	1.40+5	1.08
19	1.54+5	1.46+5	1.05
20	1.04+5	1.01+5	1.03
21	5.14+5	8.03+5	0.64
22	8.42+4	2.92+5	0.29
23	1.72+5	6.17+5	0.28
24	9.35+4	3.16+5	0.30
25	7.30+4	2.64+5	0.28
26	1.18+5	4.41+5	0.27
27	1.39+5	4.22+5	0.33
28	2.24+5	4.15+5	0.54

* Groups 1 through 21 are for the neutron and groups 22 through 28 are for gamma ray.

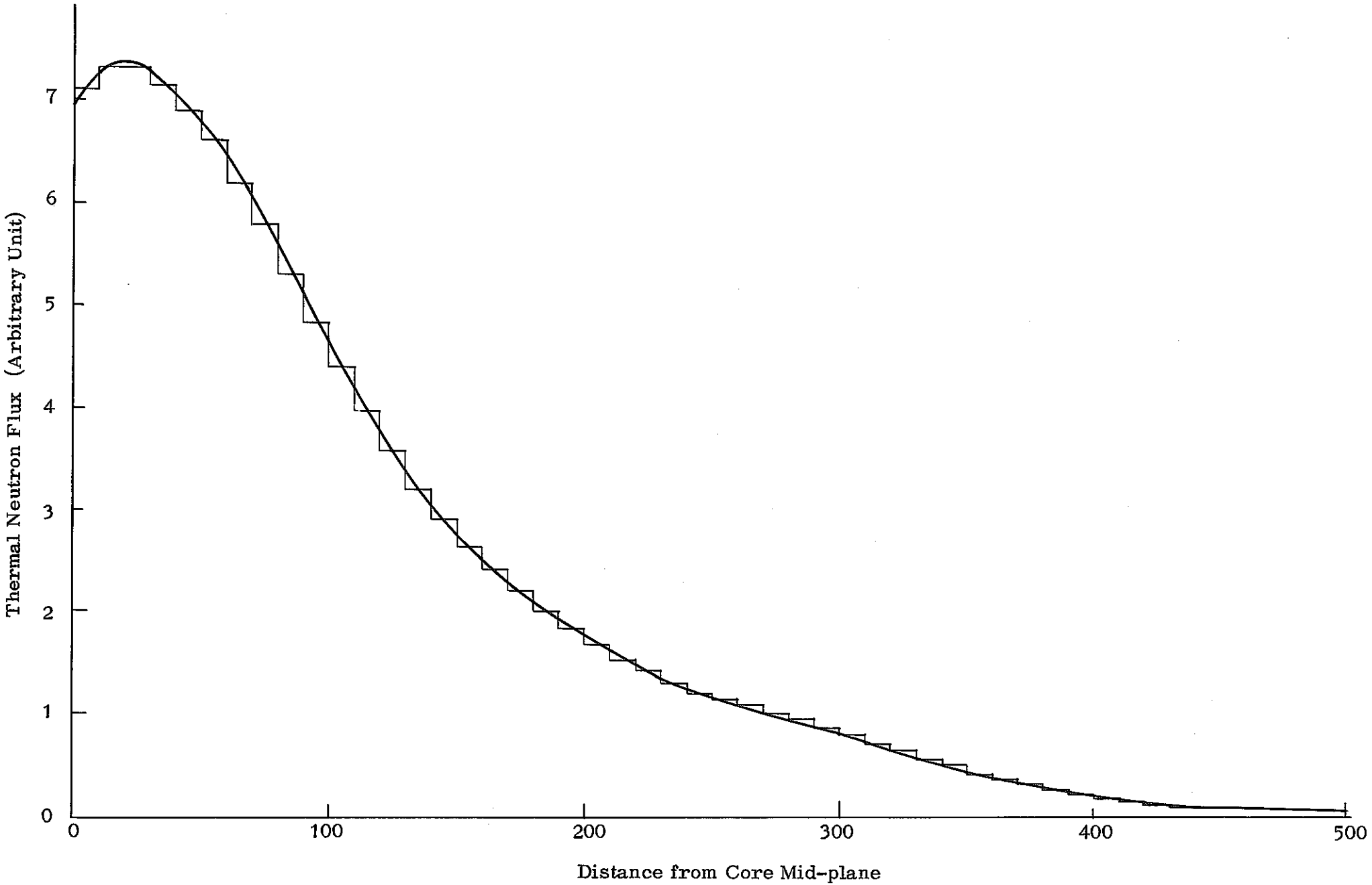

Fig.2.4.1 Assumed Thermal Neutron Flux Profile along Detector Tube

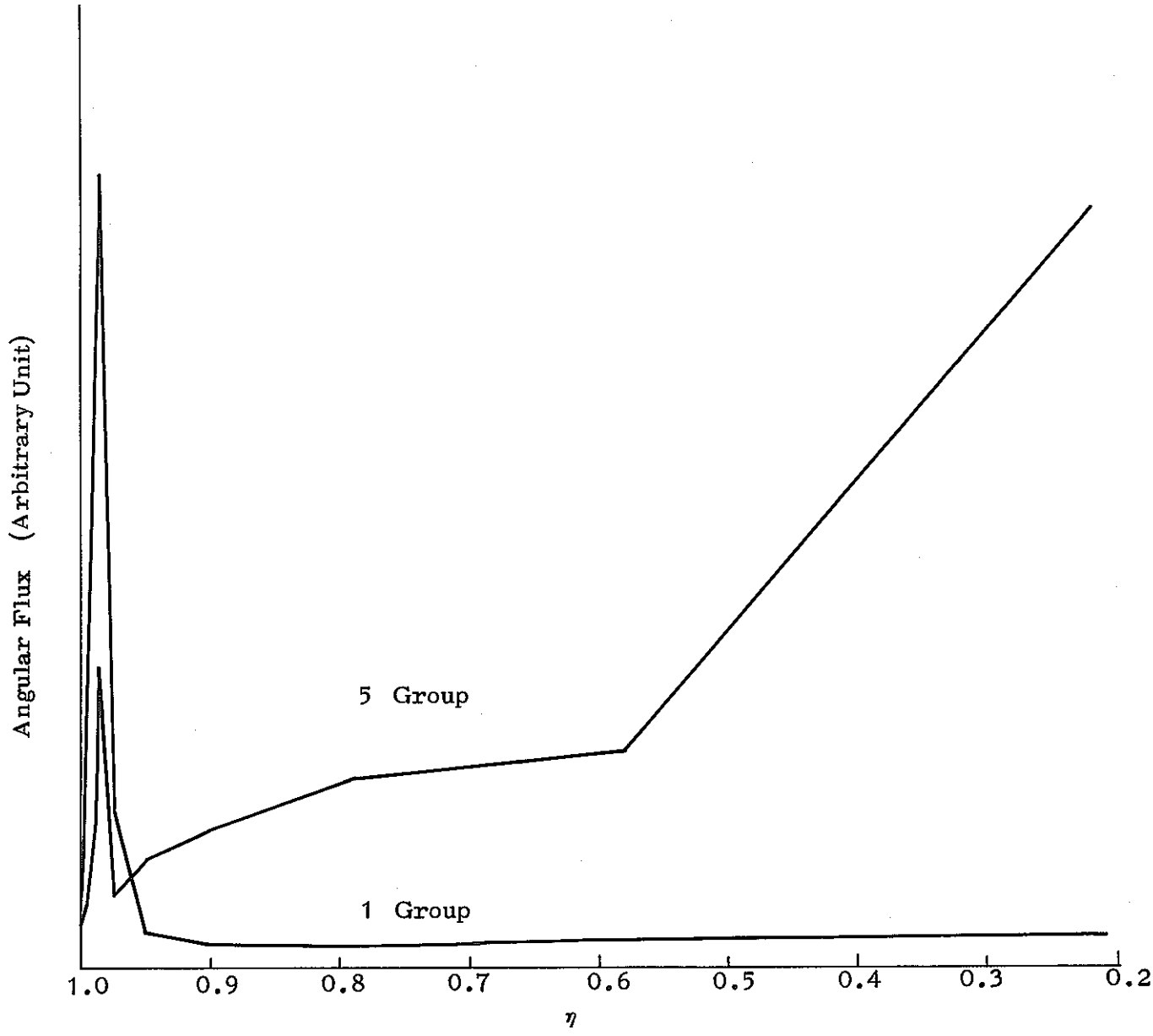

Fig.2.4.2 Schematic Angular Flux Distribution for Fast Neutron

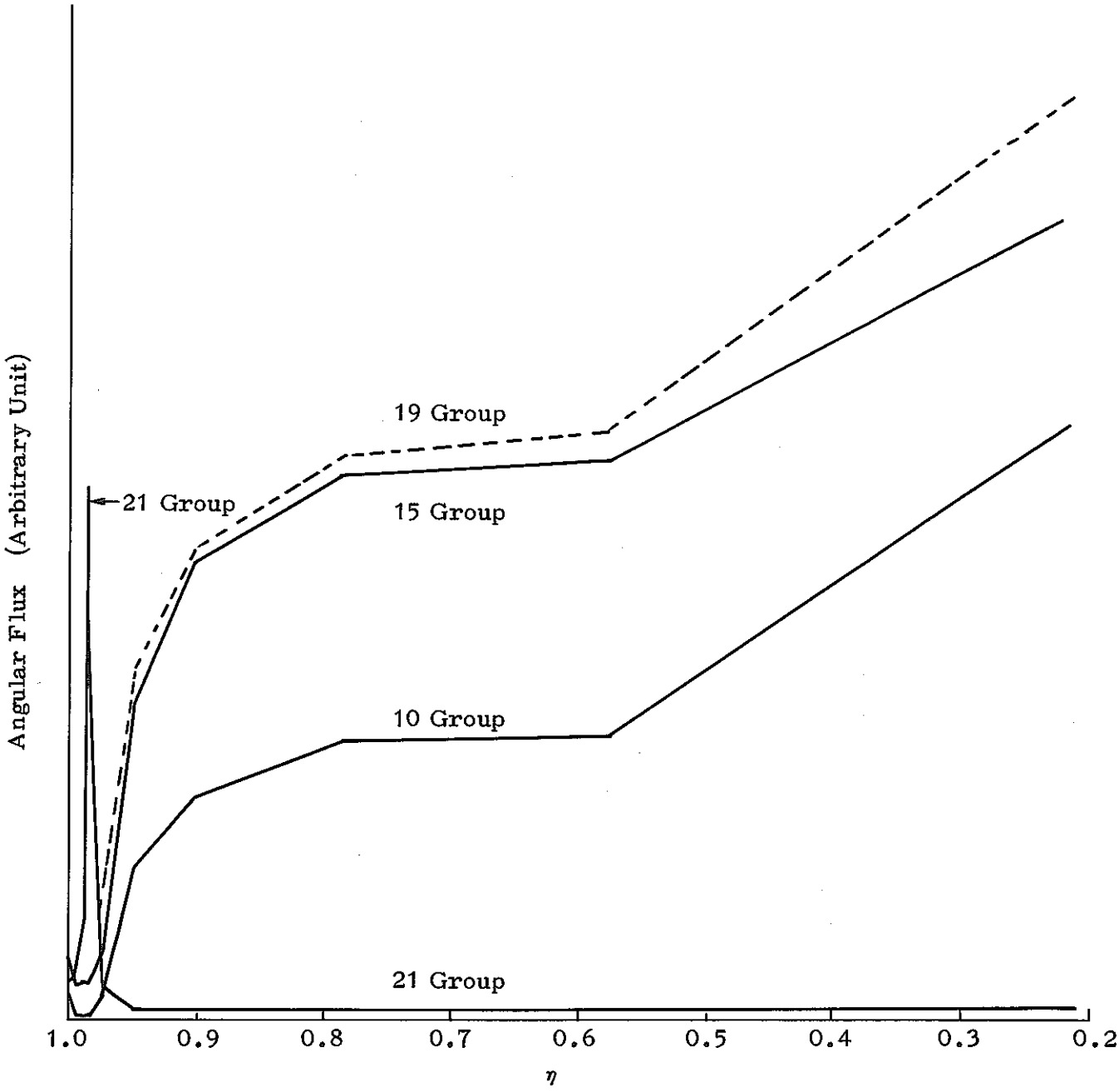

Fig.2.4.3 Schematic Angular Flux Distribution for Intermediate and Thermal Neutron

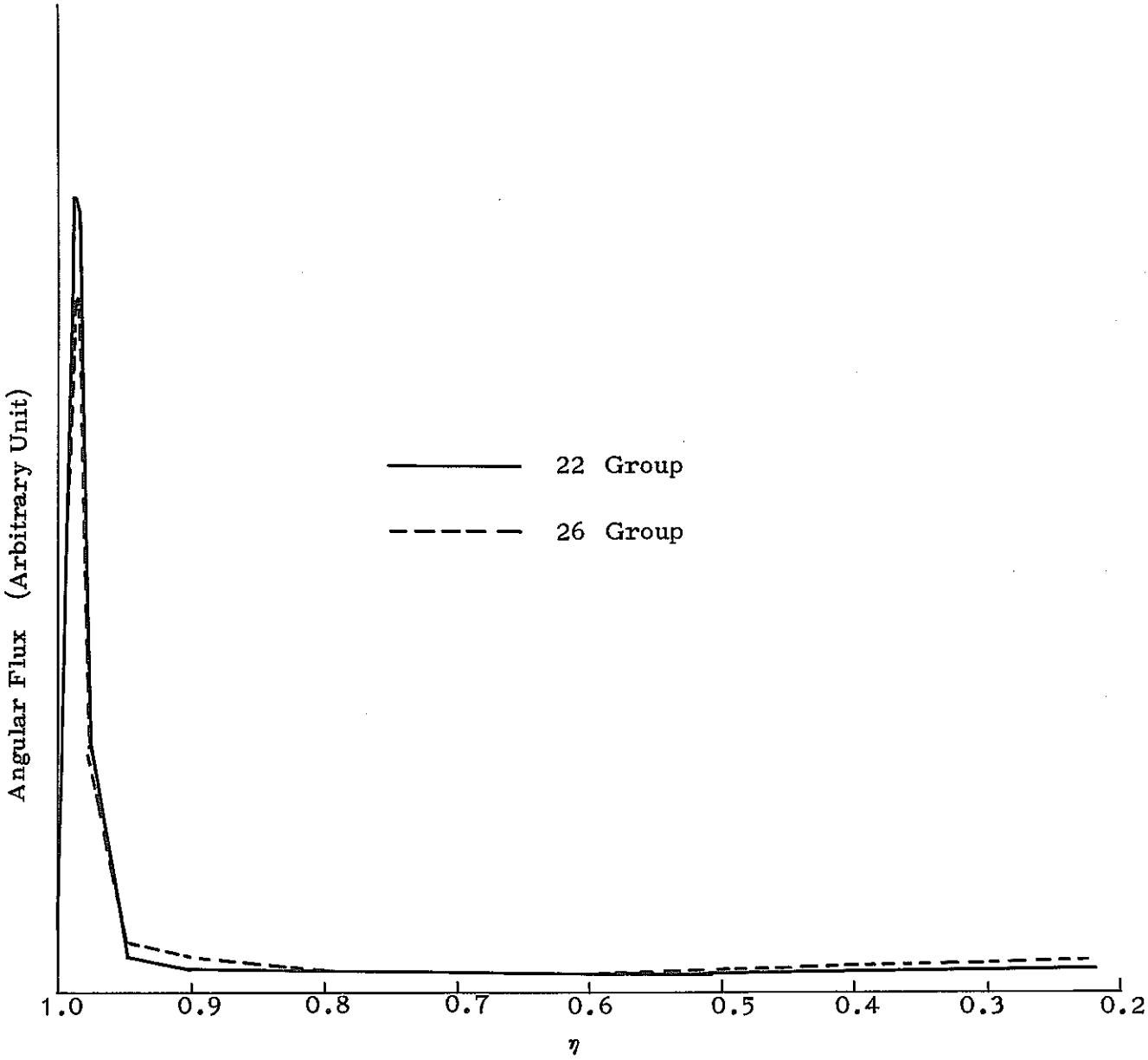

Fig.2.4.4 Schematic Angular Flux Distribution for Gamma Ray

CHAPTER 3

EVALUATION OF SODIUM ACTIVITY

3.1 Introductory remarks

Radioactivity of the primary coolant was evaluated as the effect that neutrons in a reactor vessel have on the shield design of the primary heat transport system (PHTS). The primary objective of this study is to obtain information that how much accurate we can predict the primary sodium activity by using the neutron flux distribution and spectrum calculated by our shielding analysis method.

When sodium coolant passes through a reactor, it becomes radioactive by neutron capture. The sodium activity depends on the magnitude of the neutron flux, the time of exposure and the activation cross section for the reaction. Therefore, the calculation of the sodium activity is dependent of the neutron flux distribution and the sodium flow. We will show, in section 3.2, the sodium activation is expressed in a simple form under some restrictions.

At the time the full reactor shielding analysis was initiated we focussed our attention on the neutron flux distribution in the full reactor upper axial two dimensional model. Then the lower axial two dimensional calculation was needed in this study.

The lower axial two dimensional calculation will be described in the next section followed by the description of the sodium activity evaluation method. Then the evaluated sodium activity will be discussed by comparing it with the measured value.

3.2 Full reactor lower axial two dimensional calculation

The calculation technqiue used in this section is the same as that of the previous full reactor upper axial two dimensional calculation. The geometry for the lower axial calculation is shown in Fig.3.2.1 with the regions identified in Table 3.2.1. The region extended from the center of the core to a point 15 cm into the graphite shield. The spatial mesh intervals and materials used are the same as those of the previous upper axial calculation for regions common to both geometry. The P_1 scattering cross sections were used for this calculation. Table 3.2.2 summarize the calculational parameters used in this lower axial calculation.

The calculational results are shown in Figs. 3.2.2 through Figs.3.2.4.

Table 3.2.1 Description of Regions in Full Reactor Lower Axial 2 - D Calculation

Region No.	Content	Region No.	Content
1	Inner Core	32	Entrance Nozzle
2	Control Rod	33	Core Support Upper
3	Outer Core	34	"
4	Radial Blanket	35	"
5	Removable Reflector	36	Connection Pipe
6	Sodium	37	"
7	Inner Neutron Shield	38	Sodium
8	Fuel Storage Rack	39	Outer Frame
9	Core Barrel	40	Sodium
10	Outer Neutron Shield	41	Core Support Lower
11	Sodium	42	"
12	Sodium	43	"
13	Thermal Shield	44	Connection Pipe Knot
14	Reactor Vessel	45	"
15	Nitrogen	46	Core Support
16	Leak Jacket	47	Sodium
17	Insulation	48	Bottom Plate
18	Nitrogen	49	Lower Flange
19	Graphite Shield	50	Structure
20	Axial Blanket	51	"
21	"	52	Sodium
22	Lower End Plug	53	Rib
23	"	54	Rib Plate
24	"	55	Sodium
25	Inner Core Frame	56	"
26	Outer Core Frame	57	Reactor Vessel
27	Radial Blanket Piping	58	Nitrogen
28	Entrance Nozzle	59	Reactor Vessel Structure
29	"	60	"
30	"	61	"
31	Entrance Nozzle	62	Nitrogen

Table 3.2.2 Parameters Used in Full Reactor Lower Axial 2 - D Calculation

Code	DOT3.5
Scattering	P_1
Quadrature	S - 30
Boundary conditions	Left : Reflective Right : Vacuum Bottom : Vacuum Top : Reflective
Number of material zones	62
Number of mesh intervals	Radial : 90 Axial : 87
Number of energy groups	21
General Convergence criterion	0.01
Acceleration technique	Space dependent scaling
Flux calculation model	Weighted difference mode

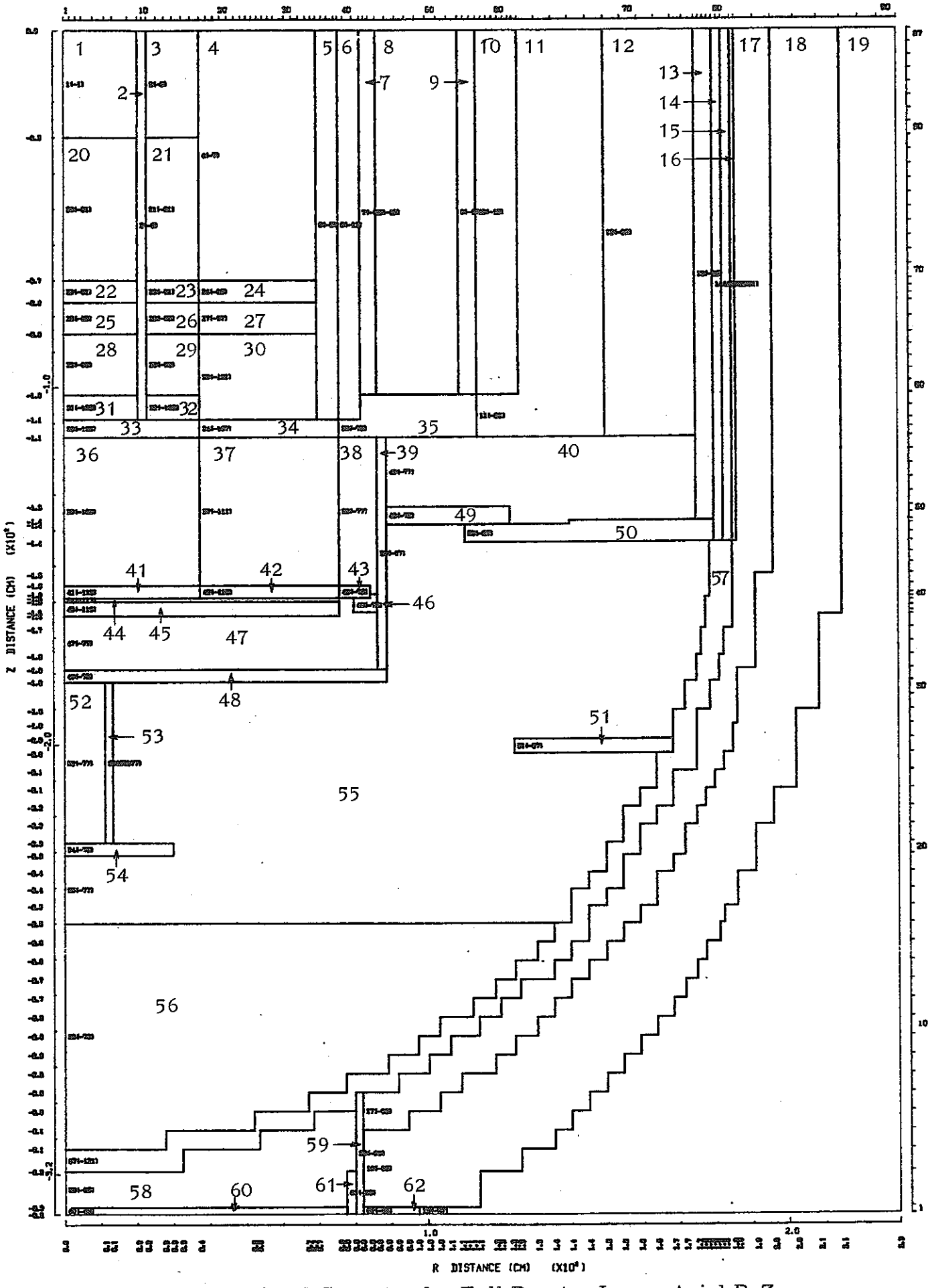

Fig.3.2.1 Calculational Geometry for Full Reactor Lower Axial R-Z Model. Refer to Table 3-1-1 for identification of regions.

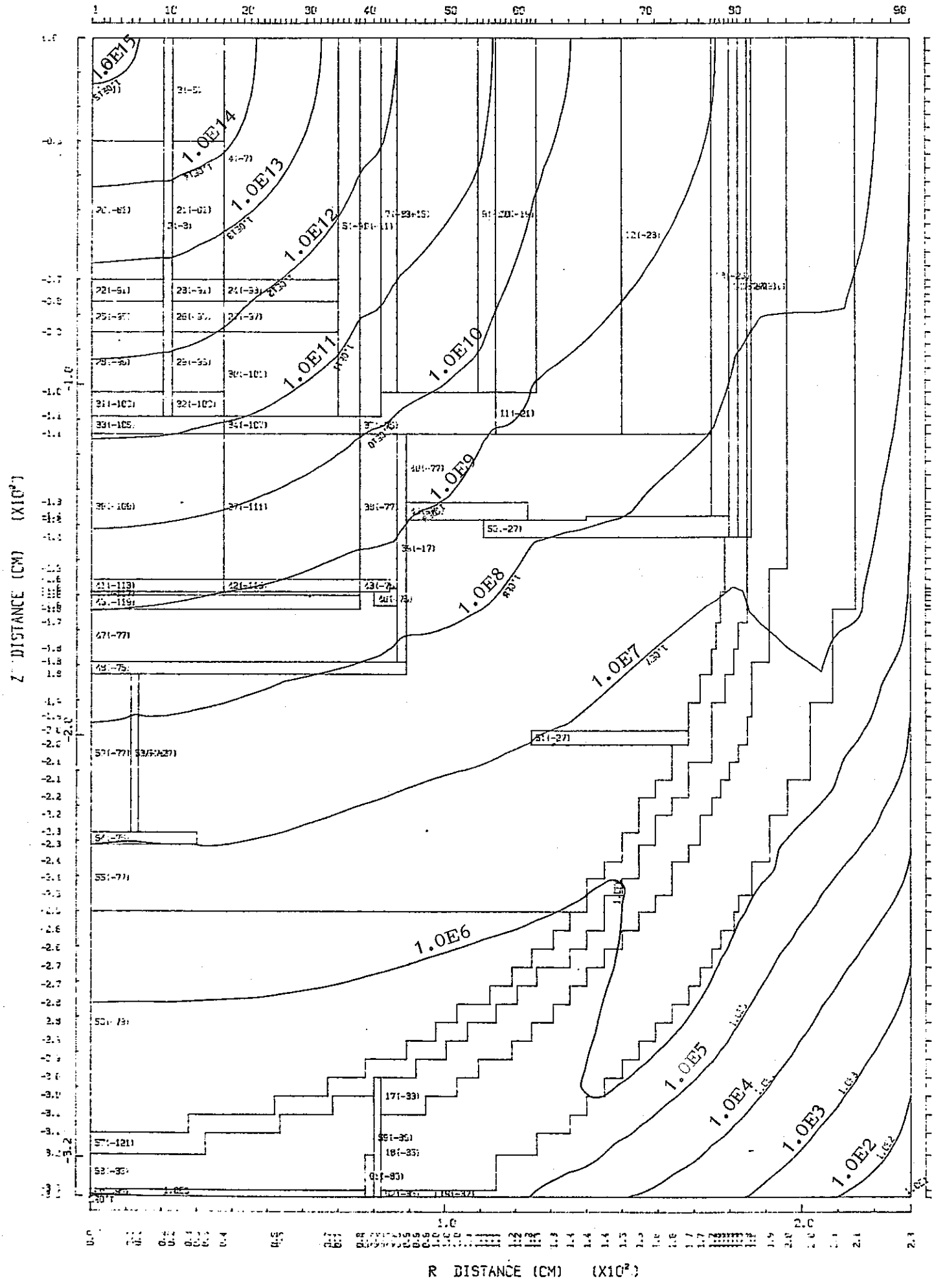

Fig. 3.2.2 Flux Distribution in Full Reactor Lower Axial Model

FAST NUETRON FLUX (N/CM**2.S) 1.4918E+07 - 7.4274E+05 (EV) (GROUP 1-5)

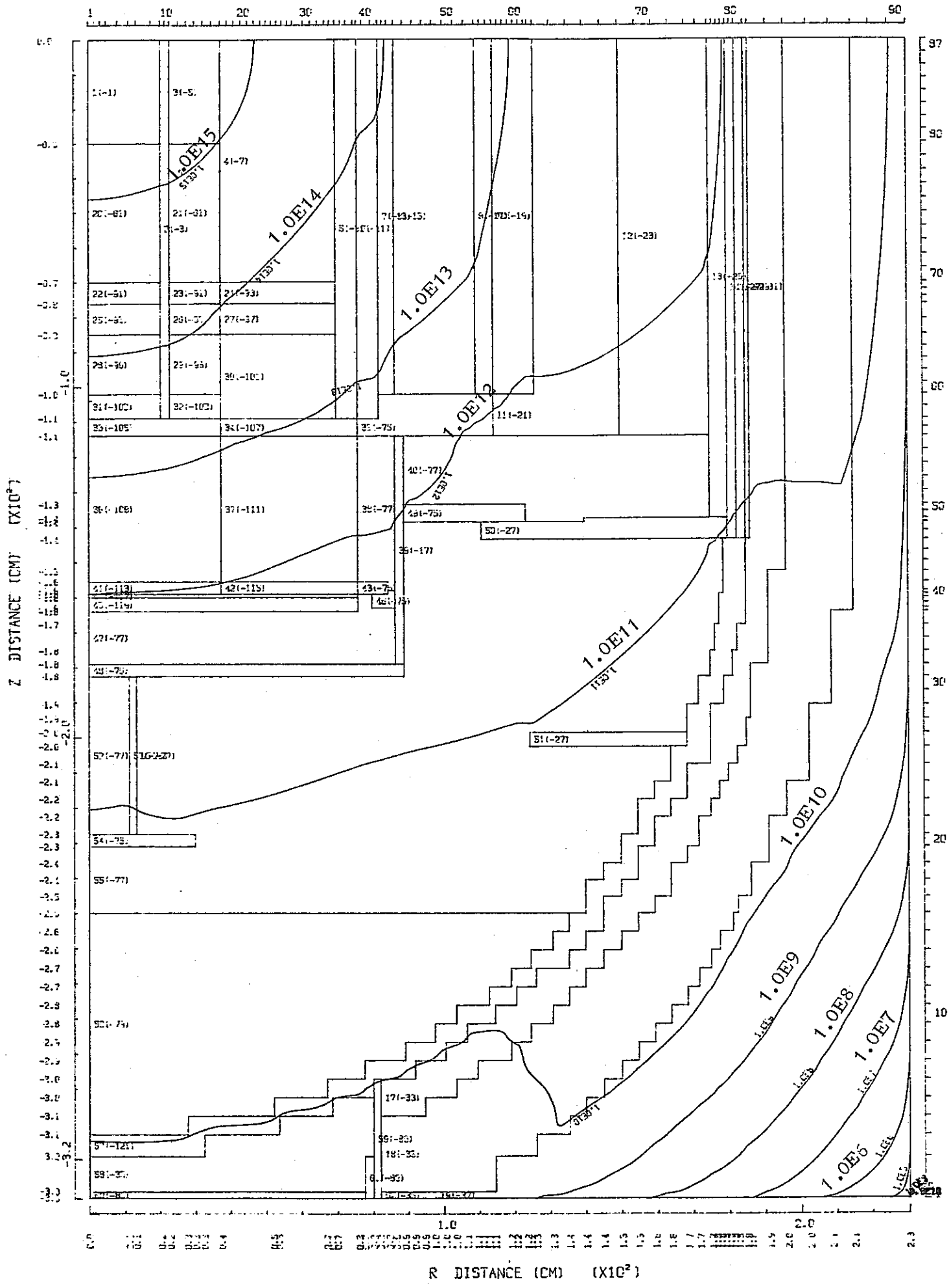

Fig.3.2.3 Flux Distribution in Full Reactor Lower Axial Model

INTERMEDIATE NUETRON FLUX (N/CM**2.S) 7.4274E+05 - 4.1399E-01 (EV) (GROUP 6-20)

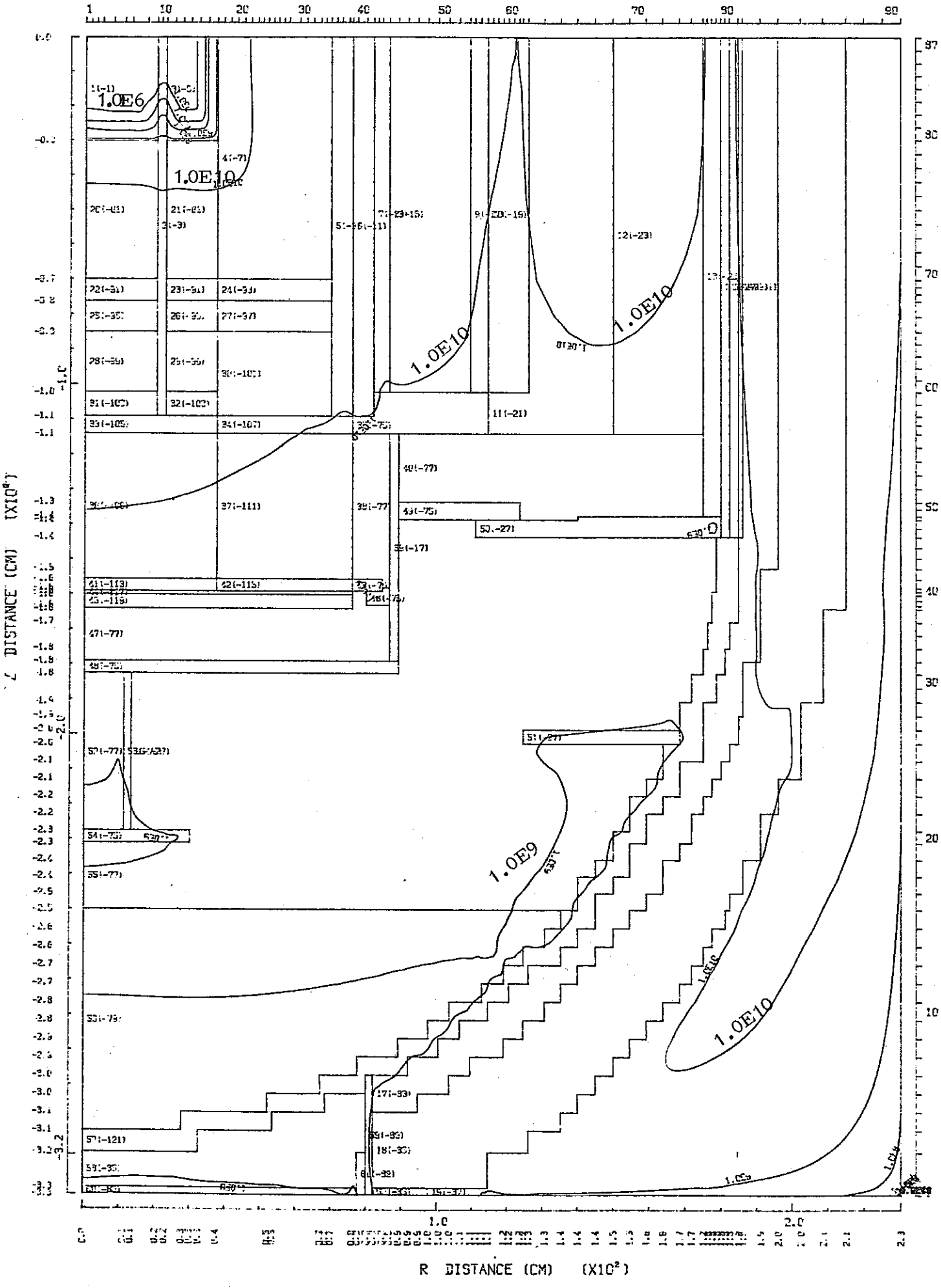

Fig.3.2.4 Flux Distribution in Full Reactor Lower Axial Model

THERMAL NUETRON FLUX (N/CM**2.S) 4.1399E-01 - 1.0000E-03 (EV) (GROUP 21-21)

3.3 Evaluation of the sodium activity

3.3.1 Evaluation Method

Sodium flow diagram in JOYO is approximated as shown in Fig. 3.3.1. There are six regions in the reactor vessel and one region corresponding to PHTS loops. When the sodium coolant flows into a lower sodium plenum it suffers neutron irradiation for t_1 seconds and is devided into two flow paths. One goes to a high pressure plenum and again devided into two flow paths respectively going to core fuel region and radial blanket region (including the outer regions to the outer neutron shield), and the other goes to outer sodium plenum. Sodium in three flow paths meets and is mixed at the upper sodium plenum. We designate t_m as the time of exposure and V_m as the sodium volume in region m. Let f_m in the figure represent the fractional flow rate normalized to $f_2 + f_5 = f_3 + f_4 + f_5 = 1$.

We assume that the sodium coolant is activated by the magnitude of Φ_m in unit of disintegration/cm^3.sec through passing the region m. Then the sodium coolant gets activity of the magnitude of

$$\begin{aligned} A_1 = \{ f_3 [(\Phi_1 e^{-\lambda t_2} + \Phi_2) e^{-\lambda t_3} + \Phi_3] \\ + f_4 [(\Phi_1 e^{-\lambda t_2} + \Phi_2) e^{-\lambda t_4} + \Phi_4] \\ + f_5 [\Phi_1 e^{-\lambda t_5} + \Phi_5] \} e^{-\lambda t_6} + \Phi_6 \end{aligned} \qquad (3.3.1)$$

during the sodium passes through the reactor, where λ is a decay constant in unit of inverse second. In deriving the above equation we assumed that the sodium is instantaneously and entirely mixed at the junction region. Considering the radioactive decay through the PHTS loops the sodium activity after the n th cycle is given by

$$A_n = A_1 \frac{1 - F^n}{1 - F} \qquad (3.3.2)$$

where

$$F = f_3 e^{-\lambda T_3} + f_4 e^{-\lambda T_4} + f_5 e^{-\lambda T_5} \qquad (3.3.3)$$

$$T_3 = t_7 + t_1 + t_2 + t_3 + t_6$$

$$T_4 = t_7 + t_1 + t_2 + t_4 + t_6$$

$$T_5 = t_7 + t_1 + t_5 + t_6$$

We now consider the activity potential Φm in region m. Let region m be devided into Im x Jm subregions $R^m_{i,j}$, each having sodium volume $V^m_{i,j}$, $i \in Im$ and $j \in Jm$. We assume that the neutron flux $\phi^m_{i,j}$ in $R^m_{i,j}$ is constant and the macroscopic activation cross section σ is constant over the region. We assume further that the sodium flows only along one direction, say j direction. Then, the sodium activity $\Phi_{i,Jm}$ at the exit of region m along the i-th flow path is given by

$$\Phi_{i,Jm} = \sum_{j=1}^{Jm} \sigma \phi^m_{i,j} (1-e^{-\lambda t_{i,j}}) e^{-\lambda \sum_{k=j+1}^{J} t_{i,k}} ,$$

where we denote $t_{i,j}$ the time of exposure in subregion $R^m_{i,j}$ In the case of $\lambda t_{i,j} \ll 1$ and $\lambda (t_{i,1} + \cdots + t_{i,J}) \ll 1$, we can rewrite

$$\Phi_{i,Jm} = \lambda \sum_{j=1}^{Jm} t_{i,j} \sigma \phi^m_{i,j}$$

Let a fraction of flow rate along i-th path in region m be f^m_i and the total flow rate M. Then

$$\Phi_m = \frac{\lambda}{M} \sum_{i=1}^{Im} \sum_{j=1}^{Jm} V^m_{i,j} \sigma \phi^m_{i,j} \qquad (3,3,4)$$

Substituting this expression into Eq. (3.3.1) and performing a simple calculation, we can obtain

$$A_n = \frac{\lambda}{M} \sum_m \sum_i \sum_j V^m_{i,j} \sigma \phi^m_{i,j} \frac{1 - F^n}{1 - F} \qquad (3.3.5)$$

$$F = 1 - \frac{\lambda}{M} \sum_{m=1}^{7} V_m \qquad (3.3.6)$$

If we define the average time for a complete cycle t_{av} as

$$t_{av} = \frac{1}{M} \sum_{m=1}^{7} V_m \quad , \tag{3.3.7}$$

then,

$$1 - F^n = 1 - (1 - \lambda\ t_{av})^n = 1 - e^{-\lambda n t_{av}}$$
$$= 1 - e^{-\lambda T}$$

where T is the time of reactor operation. Therefore, the sodium coolant activity is given by

$$A = \frac{\sum_i \sum_j V_{i,j}\ \sigma_{i,j}\ \phi_{i,j}}{\sum_m V_m}(1 - e^{-\lambda T}) \tag{3.3.8}$$

This equation is immediately applied to the result of the DOT code.

In JOYO reactor,

$t_1 = 31.1$ sec,

$t_2 = 0.98$ sec,

$t_3 = 0.84$ sec,

$t_4 = 13.7$ sec,

$t_5 = 560.7$ sec,

$t_6 = 48.1$ sec, and

$t_7 = 54.0$ sec.

The decay constant of ^{24}Na is 1.275×10^{-5} sec^{-1} and that of ^{22}Na is 8.454×10^{-9} sec^{-1}. Then we can apply Eq.(3.3.8) to predict the sodium activity.

3.3.2 Comparison of the calculated sodium activity with the measured activity

The sodium activity was calculated by using the calculational neutron flux and the activation cross section for ^{23}Na from the ENDF/B-IV.

In Fig.3.3.2 the calculated ^{24}Na activity is shown in comparison with the measured data. The calculated activity is two times larger than the measured one.

Table 3.3.1 shows the calculated ^{22}Na activity in comparison with the measured activity. The calculated activity is higher by a factor of about 1.5 than the measured activity.

More information of the calculated ^{24}Na activity is that the region from the core support to the gas plenum and from the core fuel to the outer neutron shielding produces about 90% of sodium activity. As to the neutron energy, the group 13 (corresponding to sodium resonance group) has 45% contribution to the total activity produced.

Table 3.3.1 ^{22}Na Activity as a Function of Time

Duration (day)	Accumulated Power (MWD) per Duration	Accumulated Power (MWD) Total	Average Power (MW)	^{22}Na Activity ($\mu Ci/g$) Calculated	^{22}Na Activity ($\mu Ci/g$) Measured	C/E
25	146.7	146.7	5.9	1.8×10^{-3}	-	
4	0.0	146.7	0.0	1.8×10^{-3}	-	
59	1456.0	1602.7	24.7	2.0×10^{-2}	1.2×10^{-2}	1.7
5	0.0	1602.7	0.0	2.0×10^{-2}	1.2×10^{-2}	1.7
32	833.6	2436.3	26.1	3.0×10^{-2}	1.8×10^{-2}	1.7
57	0.0	2436.3	0.0	2.8×10^{-2}	1.8×10^{-2}	1.6
56	2123.2	4559.5	37.9	5.4×10^{-2}	3.5×10^{-2}	1.5
31	0.0	4559.5	0.0	5.2×10^{-2}	3.5×10^{-2}	1.5
46	2141.2	6700.7	46.5	7.8×10^{-2}	5.6×10^{-2}	1.4
78	0.0	6700.7	0.0	7.4×10^{-2}	4.8×10^{-2}	1.5
11	164.1	6864.8	14.9	7.6×10^{-2}	4.8×10^{-2}	1.6
37	0.0	6864.8	0.0	7.4×10^{-2}	4.8×10^{-2}	1.5
52	2016.9	8881.7	38.8	9.6×10^{-2}	6.5×10^{-2}	1.5
145	0.0	8881.7	0.0	8.6×10^{-2}	5.7×10^{-2}	1.5
47	2910.5	11792.2	61.9	1.2×10^{-1}	7.8×10^{-2}	1.5
40	0.0	11792.2	0.0	1.2×10^{-1}	7.8×10^{-2}	1.5
3	13.9	11806.1	4.6	1.2×10^{-1}	7.8×10^{-2}	1.5
22	0.0	11806.1	0.0	1.1×10^{-1}	7.8×10^{-2}	1.4
48	3040.0	14846.1	63.3	1.5×10^{-1}	9.8×10^{-2}	1.5
19	0.0	14846.1	0.0	1.5×10^{-1}	9.8×10^{-2}	1.5
47	2989.5	17835.6	63.6	1.8×10^{-1}	1.2×10^{-1}	1.5
194	0.0	17835.6	0.0	1.6×10^{-1}	9.5×10^{-2}	1.7
61	3385.1	21220.7	55.5	1.9×10^{-1}	1.2×10^{-1}	1.6

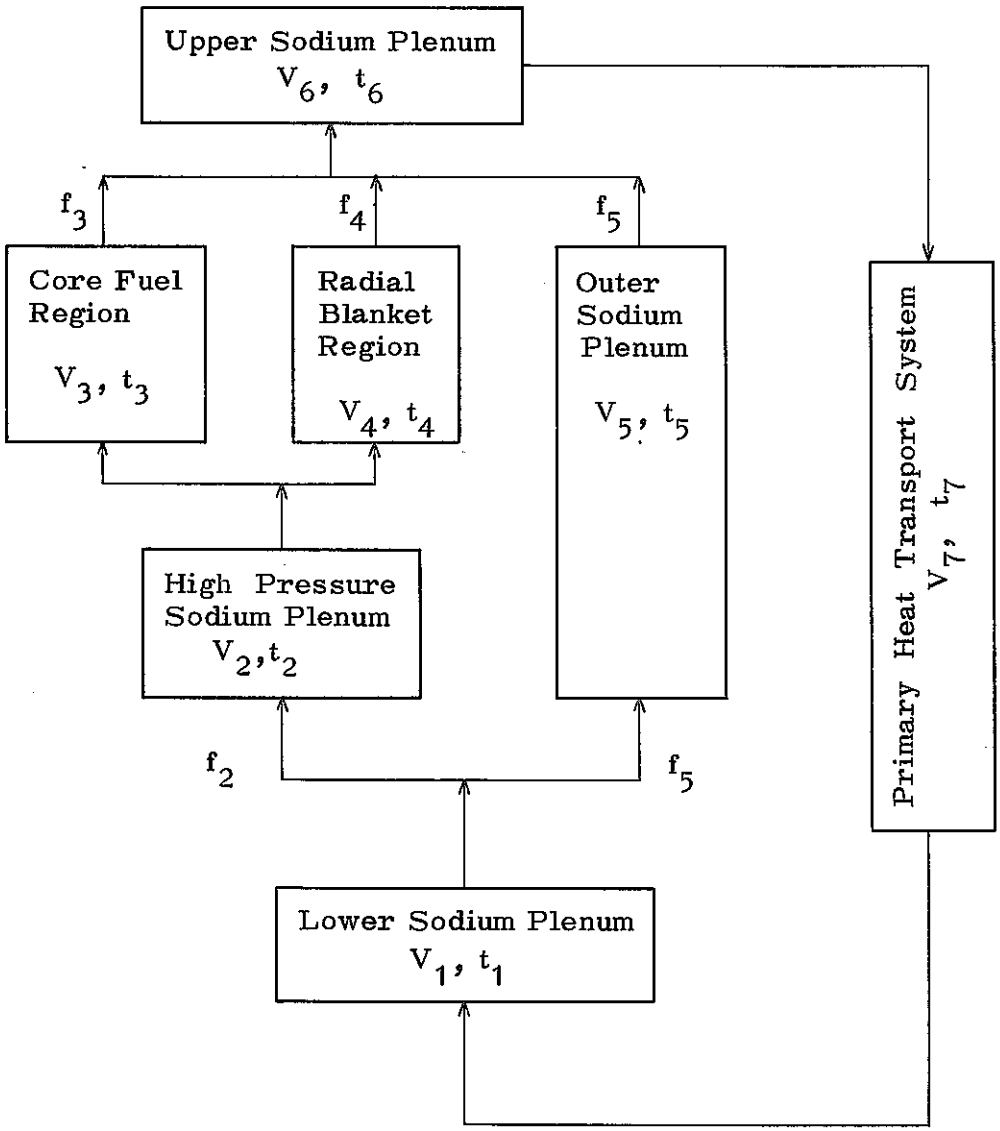

V_m : Sodium Volum (cm^3)

t_m : Time of Exposure (sec)

f_m : Fraction of Flow Rate

Fig.3.3.1 Schematic Sodium Flow Diagram in JOYO

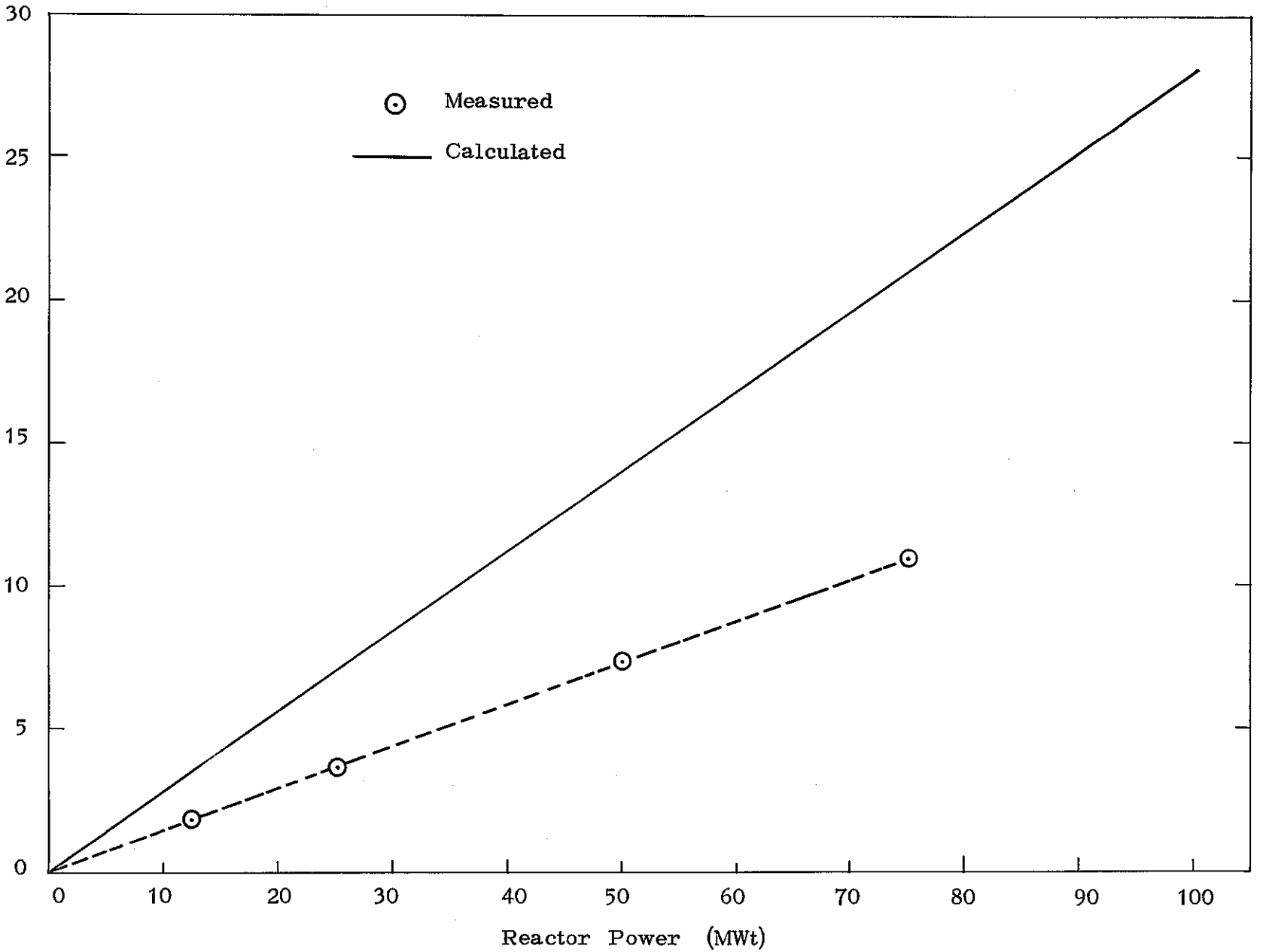

Fig.3.3.2 ^{24}Na Activity as a Function of Reactor Power

CHAPTER 4

CONCLUDING REMARKS

4.1 The effect of the guide tube on the neutron flux and the gamma ray dose rate

The most significant results of the analysis for the effect of the guide tube in the graphite shielding are summarized as follows :

(1) The gamma dose rates along the guide tube obtained from the calculational model with the guide tube taken into account are as about fifteen times as higher than those from the model neglecting the guide tube.

(2) The guide tube gives no significant effect on the neutron flux.

(3) The C/E values are in the range from 0.3 to 1.5 for the gamma dose rate and in the range from 1.7 to 3.8 for the thermal neutron flux.

(4) If we could correct the source strength of the secondary gamma ray by using the C/E values for the thermal neutron flux, the C/E value for the gamma ray dose rate would be about 0.25 which is still much better than that of the full reactor shielding analysis.

(5) The gamma ray dose rate along the guide tube is dominated by the secondary gamma ray from the guide tube. Therefore, the effect of the guide tube should not be neglected when performing the comparison between calculation and measurement.

The effect of the guide tube penetrating the heavy concrete pedestal is apparently the streaming particularly on the neutron flux. The C/E values for the thermal neutron flux along the guide tube are in the range from 3.0 to 8.0, which were well improved comparing with the C/E values in the range from 5.6×10^{-3} to 0.15 obtained from the full reactor shielding analysis. The C/E values for the gamma ray dose rate

are also improved comparing with the result of the full reactor analysis. We should give attention to the streaming effect when comparing the data between calculation and measurement.

As to the simple analytical method we can conclude that the method used in this study for the guide tube penetrating the graphite shield gives a fairly good result and that we can approach the similar problem to that in this study. For the guide tube penetrating the heavy concrete pedestal, however, the simple streaming analysis gives the underestimation. An analytical method incorporating the angular distribution of the entrance flux are thought to give a good result.

4.2 Sodium activity Evaluation

The ^{24}Na activity using the calculated neutron flux is 14 mCi/gNa at the reactor power of 50 MW, while the measured activity is 7.3 mCi/gNa. For the ^{22}Na activity, the calculated value is higher by a factor of 1.5 than the measured activity. Although the calculated activity does not give the underestimation, the difference between the calculated and measured activity seems to be larger than expected. Therefore, the more detail analysis for the sodium activity should be performed in the future.

REFERENCES

1) PNC, "Radiation Shielding Analyses of JOYO," SN 241 81-29 (Nov. 1981).

2) T. Hikichi and Y. Sato, "Fission Product and Corrosion Product Distribution," SA013 81-01(8) PNC (April 1981).

3) A. Simon and C.E. Clifford, "The Attenuation of Neutrons by Air Ducts in Shields," Nucl. Sci, Engi., 1, 156-166 (1956).

4) W.A. Rhoades and F.R. Mynatt, "The DOT III Two-Dimensional Discrete Ordinates Transport Code," ORNL-TM-4280 (Sept. 1973).

ACKNOWLEDGEMENT

It is a pleasure to thank Dr. N. Ohtani for many helpful discussions and suggestions. Thanks are also to Mr. T. Hikichi and Mr. S. Suzuki for presenting many shielding data of JOYO.